A Comparison of Wave Spectra Reconstruction Methods

Xinyi Zhang

Delft University of Technology

TU Delft

A comparison of wave spectra reconstruction methods

Xinyi Zhang

February 2022

An additional thesis submitted for the course CIE5050-09 Additional Graduate Work, Research Project (2021-2022)

Supervisors: Dr. Marion Tissier — Delft University of Technology
Dr. Jantien Rutten — Delft University of Technology
Dr. Yoshinao Matsuba — IHE Delft Institute for Water Education

Xinyi Zhang: *A comparison of wave spectra reconstruction methods* (2022)
Student Number: 5217903
An electronic version of this thesis is available at https://repository.tudelft.nl.

Acknowledgements

This additional thesis serves as part of the curriculum of the master's degree in Civil Engineering at Delft University of Technology. The thesis tested several wave spectra reconstruction methods in sea-swell and infragravity wave fields.

I would like to thank my supervisors Marion Tissier, Jantien Rutten, and Yoshinao Matsuba, for their support during this project. I would like to thank Marion for providing me with this opportunity to work on this project, her advice is appreciated very much. I would like to thank Jantien for her patience and advice in our weekly meetings and her feedback on the report, I also appreciate her hospitality when I visited the REFLEX field experiment. I also want to express my gratitude to Yoshi for sharing the wave generation code and his insights on this topic, without him, this work would be much harder to complete. Thank you all for your guidance, this means a lot to me.

Xinyi Zhang

Delft, February 2022

Abstract

Infragravity (IG) waves are long waves whose frequency ranges between 0.005 Hz to 0.04 Hz. The directional properties of IG waves are essential in various engineering fields, but few spectra reconstruction methods have been tested to be robust for the last forty years. In this study, artificial wave signals were created to check the accuracy and reliability of several wave spectra reconstruction methods. These data were designed as if produced from the REFLEX field measurements. Three commonly used conventional directional wave spectra reconstruction methods, EMEP, IMLM and BDM, are applied and compared over Sea-swell (SS) wave field and IG+SS wave field.

Though the existence of bound IG waves weakens the accuracy and reliability of these methods, they may be used to reconstruct the IG wave spectra with reasonable results. It is found that the EMEP outperforms the BDM and the IMLM since it yields accurate results with low sensitivity to noise in most cases. The BDM is realiable in moderate wave conditions, but would fail in case of high wave height or narrow directional spreading. The IMLM tends to produce less accurate results than the EMEP. The EMEP is recommended because of its overall reliability and low sensitivity.

Contents

1 Introduction **1**

2 Literature Review **5**

2.1 Measurment of Directional Wave Data 5

2.2 Directional Wave Spectrum 6

2.3 Directional Wave Analysis 7

2.4 Review of Existing Reconstruction Methods 9

2.4.1 Open Ocean Wave Fields 9

2.4.2 Reflective Wave Fields 10

2.4.3 Directional Wave Spectra Reconstruction of IG Waves 11

2.4.4 REFLEX Measurement Campaign 12

2.5 Research Objectives and Research Questions 13

3 Methodology **15**

3.1 Introduction 15

3.2 Data Preparation 15

3.3 DIWASP 19

3.3.1 Working Procedure 19

3.3.2 Reconstruction Methods 19

4 Results **23**

4.1 Analyzed Results of SS Waves 23

4.1.1 Benchmark Tests 23

4.1.2 Sensitivity Tests 26

4.1.3 Special Issues Regarding the BDM 28

4.2 Analyzed Results of IG Waves 31

4.2.1 Free IG Wave Fields 31

4.2.2 Bound IG Wave Fields 34

5 Discussion **41**

5.1 Single-Point Systems 41

5.2 Energy Discrepancy between Spectral Parameters and Generated Spectra 42

5.3 Recommendations 42

6 Conclusions **43**

List of Figures

2.1 Velocity ratio of 1D bound and free IG waves. (van Essen et al., 2013) 12

3.1 Flow chart showing the working process 20

4.1 Analyzed results for $H_s = 2.5m, T_p = 6s$, water depth = 14m, compared with the original spectrum (3D visualization). 24

4.2 Analyzed results for $H_s = 2.5m, T_p = 6s$, water depth = 14m, compared with the original spectrum. 24

4.3 Analyzed results for $H_s = 3.25m, T_p = 8s$, water depth = 14m, compared with the original spectrum. 25

4.4 Analyzed results for $H_s = 4m, T_p = 10s$, water depth = 14m, compared with the original spectrum. 25

4.5 %Error when changing noise level. $H_s = 3.25m, T_p = 8s$, water depth = 14m, for EMEP (red), BDM (magenta) and IMLM (blue). 26

4.6 %Error when changing location of the velocity measurement, counted from the sea floor. $H_s = 3.25m, T_p = 8s$, water depth = 14m, for EMEP (red), BDM (magenta) and IMLM (blue). 26

4.7 %Error when changing significant wave height or peak period, water depth = 14m, (a): keep $T_p = 8s$, change significant wave height H_s; (b): keep $H_s = 3.25m$, change significant wave height T_p, for EMEP (red), BDM (magenta) and IMLM (blue). 27

4.8 (a): The relation between the directional width σ and the spreading factor in $\cos^{2s}$ model; (b): %Error when changing spreading factor s, $H_s = 3.25m, T_p = 8s$, water depth = 14m, for EMEP (red), BDM (magenta) and IMLM (blue). 28

4.9 Analyzed results from the BDM, compared with the original spectrum, $H_s = 3.25m, T_p = 8s$, water depth = 14m. (a), (b): $\sigma = 10°$; (c), (d): $\sigma = 30°$, for original (dashed line), EMEP (red), BDM (yellow) and IMLM (blue). 29

4.10 Analyzed results at the peak frequency, compared with the original spectrum, $H_s = 3.25m, T_p = 8s$, water depth = 14m. (a): $\sigma = 10°$; (b): $\sigma = 30°$, for original (dashed line), EMEP (red), BDM (yellow) and IMLM (blue). 29

4.11 Analyzed results from the BDM, compared with the original spectrum, $\sigma = 20°$. (a), (b): $H_s = 2.5m, T_p = 6s$, water depth = 8m; (c), (d): $H_s = 4m, T_p = 6s$, water depth = 14m. 30
4.12 Analyzed results at the peak frequency, compared with the original spectrum. (a): $H_s = 2.5m, T_p = 6s$, water depth = 8m; (b): $H_s = 4m, T_p = 6s$, water depth = 14m, for original (dashed line), EMEP (red), BDM (yellow) and IMLM (blue). . . 31
4.13 Analyzed results at different frequencies, compared with the original spectrum, $H_s = 3.25m, T_p = 8s$, water depth = 14m, bound waves are not included. (a)-(e): directional spreading function at different frequencies; (f): Directional spreading function, integrated over IG frequency range 0.005-0.04 Hz, for original (dashed line), EMEP (red), BDM (yellow) and IMLM (blue). 32
4.14 Analyzed results for white noise only, same case as before, the noise level is 0.2. (a): The directional spreading function, integrated over IG frequencies; (b): The directional spreading function, integrated over all frequencies, for original (dashed line), EMEP (red), BDM (yellow) and IMLM (blue). 33
4.15 The relative contribution of bound IG waves R^2, $T_p = 8s$; star: water depth = 14m; square: water depth = 8m. 34
4.16 Analyzed results at different frequencies, compared with the original spectrum, $H_s = 2m, T_p = 8s$, water depth = 14m. Left: only free waves; Right: bound IG waves included, for original (dashed line), EMEP (red), BDM (yellow) and IMLM (blue). 35
4.17 Analyzed results at different frequencies, compared with the original spectrum, $H_s = 4m, T_p = 8s$, water depth = 14m. Left: only free waves; Right: bound IG waves included, for original (dashed line), EMEP (red), BDM (yellow) and IMLM (blue). 36
4.18 Analyzed results at different frequencies, compared with the original spectrum, $H_s = 4m, T_p = 8s$, water depth = 8m. Left: only free waves; Right: bound IG waves included, for original (dashed line), EMEP (red), BDM (yellow) and IMLM (blue). 37
4.19 Analyzed results at different frequencies, compared with the original spectrum, $H_s = 3.25m, T_p = 8s$, water depth = 14m, mean direction of incident free IG waves is 15°. Left: only free waves; Right: bound IG waves included, for original (dashed line), EMEP (red), BDM (yellow) and IMLM (blue). 38
4.20 Analyzed results at different frequencies, compared with the original spectrum, $H_s = 3.25m, T_p = 8s$, water depth = 14m, mean direction of incident free IG waves is 45°. Left: only free waves; Right: bound IG waves included, for original (dashed line), EMEP (red), BDM (yellow) and IMLM (blue). 39

List of Tables

3.1 Overview of tests with SS waves. 17
3.2 Overview of the sensitivity tests. 18
3.3 Overview of tests with IG waves 18

5.1 %Error of the EMEP and the BDM reconstruction for reference test cases, ”before” indicates the original results while ”after” indicates the results after considering pressure signals. 41

1 Introduction

Infragravity (IG) waves, or long waves, surf beats, low-frequency waves, are ocean surface gravity waves with frequencies ranging between 0.005 Hz to 0.04 Hz. The generation, propagation, and transformation of IG waves have always been an active research field since they were observed from the field (Munk, 1949). Bertin et al. (2018) gave an elaborated review on the driving mechanisms and impacts of IG waves, which is an excellent introduction to the state-of-the-art of IG waves-related investigations.

Generally, the IG waves are relatively insignificant in the deep ocean. However, they could become more energetic than sea-swells (SS waves, frequency range 0.04-0.3 Hz) in shallower nearshore areas (Elgar et al., 1992). Hence, the influence of IG waves can be dominant in various engineering fields. For example, dune overwash (Lashley et al., 2019), and vessel motions (Waals, 2009). van Dongeren et al. (2016) provided a review mainly focused on IG wave dynamics over coral reefs and the consequences of these waves for port operations.

Most IG waves are generated because of incident wave groups, different explanations of their origin exist, see Bertin et al. (2018). Theoretically, two wave components with minor frequency differences (f and $f + \Delta f$) generate a forced wave component with a low frequency Δf (Hasselmann, 1962). The bound wave component does not follow the linear wave theory, its wavenumber $\boldsymbol{k_{bound}}$ is the vector summation of two wavenumbers of the exciting waves $\boldsymbol{k_1}$ and $\boldsymbol{k_2}$, i.e.:

$$\boldsymbol{k_{bound}} = \boldsymbol{k_2} - \boldsymbol{k_1} \tag{1.1}$$

The wave celerities of these bound waves c_{bound} can be written as:

$$c_{bound} = 2\pi\Delta f / k_{bound} \tag{1.2}$$

Combinations of those primary waves may lead to numerous different bound wavenumbers and velocities for the same frequency Δf.

The forced IG waves, however, only account for a small part of the observed spectrum $E(\Delta f)$,

especially when the wave energy is low (Okihiro et al., 1992). It has been known that the free infragravity waves, which can be generated from non-linear processes near the shoreline, are significant in infragravity frequency ranges (Herbers et al., 1994). Moreover, free IG waves can also originate from coasts far away. Elgar et al. (1992) showed these waves from distant sources are small compared to the locally generated waves, according to long-term observations from three points at 8m or 13m depth near North Carolina, USA. Recently, Rijnsdorp et al. (2021) used a spectral wave model to show the free IG waves from remote sources in the North Sea are however not negligible during storms, these free waves could contribute to coastal dynamics.

The IG wave height is dependent on local SS conditions, more energetic SS lead to a more significant IG response. The ratio of forced and free IG waves varies based on different wave conditions and site locations. The wave energy of forced IG waves depends on the directional spectra and water depth, whereas free wave energy may also be related to adjacent topography. Herbers et al. (1995) have found that the relative contribution of forced IG waves increases with shallower water or more energetic SS waves. Reniers et al. (2021) analyzed observation data in the North Sea, and found that the relative contribution of bound IG waves to the total IG variance changes dramatically, depending on the observation site and storm conditions. The prediction of bound IG waves and their relative contribution to total IG wave height is complicated, more investigations on this regard are needed.

Wave field properties must be retrieved from the field data to tackle the aforementioned problem. The directional wave spectra are essential products since they express the directional characteristics of the wave field. Significant efforts have been dedicated to developing directional wave spectra reconstruction methods for more than forty years, but we have not reached a robust method yet.

Different reconstruction methods solve the governing equation differently, and they have their advantages or drawbacks. To get acceptable engineering solutions, it is not advised to only rely on one description of the spectra shape (Hauser et al., 2005). In other words, different methods of measurements and analysis techniques may be applied and compared to find reasonable estimations of wave directional spectra.

The importance of IG waves has been emphasized, estimating the directional wave spectra of IG waves then becomes necessary. Unfortunately, few investigations have focused on the wave directional spectra reconstruction in the IG wave field. For IG wave fields, existing methods only assume free waves, but bound waves are generally not negligible in shallow water, especially in the IG frequency domain. This gives more challenges to reconstructing the directional waves spectra of IG wave fields.

This research aims to discuss the performance of conventional directional spectra reconstruction methods for SS and IG wave fields, and this will be achieved by analyzing synthetic data time series. The reasoning and detailed description of this approach will be given in the following chapters.

In this report, a literature review is given in Chapter 2, the research objectives and the research questions are determined. Chapter 3 describes the methodology adopted in the research. Then, the analyzed results for SS wave field, SS and IG wave field are in Chapter 4. Chapter 5 discussed the obtained results and proposed some recommendations for further research. The main findings of this study are concluded in Chapter 6.

2 Literature Review

In this chapter, the theoretical background of directional wave spectrum, wave spectrum reconstruction methods are briefly reviewed. The research objectives and the research questions are shown at the end of this chapter.

2.1 Measurment of Directional Wave Data

The 2D directional wave spectra can be reconstructed from the time series of wave properties, for instance, the surface elevation and two orthogonal slopes of the water surface at one point or the surface elevations collected by three or more wave gauges. These required wave properties can be collected using different types of measurement instruments such as wave buoys or wave staffs.

The field measurement technique has been developed substantially over the last fifty years. Different types of measuring devices are available to collect data for the estimation of the directional wave spectra. The existing measuring devices may be categorized as follows (Benoit et al., 1997).

1. **Single-point systems**. The single-point systems measure the wave properties at one specific location simultaneously—generally, this kind of device record three wave signals. For example, the traditional heave-pitch-roll buoys collect water surface elevation and two orthogonal slopes of the water surface. The Acoustic Doppler Current Profilers (ADCP) are single-point systems that record the water surface elevation and two orthogonal orbital velocity components. Pressure signals can be recorded as well. Other combinations are possible, for example, 3D current meters and buoys that record three displacements or accelerations.

2. **Gauge arrays**. The gauge arrays measure wave properties from several probes located at different sites. They usually collects water surface elevations, and the spatial arrangement of the sensors highly affects the quality of the reconstructed wave spectra (Benoit and Goasguen, 1999).

3. **Remote-sensing systems**. Remote sensing techniques measure the wave properties by making a ”picture” of the wave field over a certain area. These techniques are based

on spatial correlations, instead of time correlations, as the single-point systems and the gauge arrays do. They have been applied more and more in recent years. However, this is beyond the scope of this report.

In this report we mainly consider the temporal analysis of wave signals recorded from single-point systems.

2.2 Directional Wave Spectrum

A directional energy spectrum describes the properties of the wave field at a specific place, it can be noted as $E(f,\theta)$ (Unit: $N \cdot m^{-1} \cdot Hz^{-1} \cdot rad^{-1}$), which is a function of frequency f and propagation direction θ. The directional variance spectrum $S(f,\theta)$ (Unit: $m^2 \cdot Hz^{-1} \cdot rad^{-1}$), however, is more often used in the scientific literature. The relation between $S(f,\theta)$ and $E(f,\theta)$ is defined as:

$$S(f,\theta) = E(f,\theta)/\rho g \tag{2.1}$$

Where ρ is the water density (for seawater, ρ is around 1025 kg/m^3) and g is the gravitational acceleration, approximately 9.81 m/s^2.

The decomposition of the directional variance spectrum is often carried out in literature:

$$S(f,\theta) = E(f) \cdot D(f,\theta) \tag{2.2}$$

in which E(f) is the one-dimensional variance spectrum, it can also be written in the following form:

$$E(f) = \int_0^{2\pi} S(f,\theta)\,\mathrm{d}\theta \tag{2.3}$$

The directional spreading function (DSF) $D(f,\theta)$ is a function of wave frequency and wave propagating direction. This function must suffice two conditions, as specified below:

$$D(f,\theta) \geq 0,\ \theta \in [0,2\pi] \tag{2.4}$$

$$\int_0^{2\pi} D(f,\theta)\,\mathrm{d}\theta = 1 \tag{2.5}$$

$D(f,\theta)$ describes the directional spreading of the wave energy over all directions at each frequency, the directional analysis of wave spectra is then considered to estimate the variance spectrum and the directional spreading function. The most critical part of the directional wave spectra estimation is to determine $D(f,\theta)$ from the data collected from the measuring devices.

2.3 Directional Wave Analysis

The wave field can be seen as a composition of a large number of sine waves. The instantaneous water surface elevation reads:

$$\eta(x,y,t) = \sum_{m=1}^{M} a_m \cos\left[k_m(x\cdot\cos\theta_m + y\cdot\sin\theta_m) - \omega_m t + \phi_m\right] \tag{2.6}$$

Here the surface elevation η is a superposition of a large number of sine waves, the amplitude of these sine waves are expressed as a_m. ω_m is the angular frequency and k_m is wave number. The direction is θ_m and the phases of these elementary waves are ϕ_m. Assume the linear dispersion relationship holds for all these sine waves (note d represents water depths):

$$\omega_m^2 = g k_m \tanh\left(k_m d\right) \tag{2.7}$$

The random phase model is applied, i.e., the phase ϕ_m randomly distributed over all directions. Thus we assume all the wave components are independent. The following relationship is then valid:

$$\sum_{f}^{f+\mathrm{d}f}\sum_{\theta}^{\theta+\mathrm{d}\theta}\frac{1}{2}a_m^2 = S(f,\theta)\,\mathrm{d}f\mathrm{d}\theta \tag{2.8}$$

The water surface elevation $\eta(x,y,t)$ can also be expressed in continuous form, also using the equation above:

$$\eta(x,y,t) = \int_0^{\infty}\int_0^{2\pi}\sqrt{2S(f,\theta)\,\mathrm{d}f\mathrm{d}\theta}\ \cdot\ \cos\left[k(x\cdot\cos\theta + y\cdot\sin\theta) - 2\pi f t + \phi\right] \tag{2.9}$$

Assume we use a measuring device consisting of N probes, each probe collects a certain type of wave properties, for example, surface elevation, velocity, pressure, noted as $P_n(t)$ (n varies

from 1 to N). The locations of these probes are expressed as $\boldsymbol{x_n}$ relative to the origin point, which can be defined arbitrarily. The measurement duration is T with a time step Δt. The cross-spectra between two wave signals say $(P_m; P_n)$ is defined by

$$G_{mn}(f) = \int_{-\infty}^{+\infty} R_{mn}(\tau) \mathrm{e}^{-i2\pi f\tau} \, \mathrm{d}\tau \tag{2.10}$$

with

$$R_{mn}(\tau) = \lim_{T\to\infty} \frac{1}{T} \int_0^T P_m(t) \cdot P_n(t+\tau) \, \mathrm{d}t \tag{2.11}$$

Practically, $G_{mn}(f)$ is calculated based on Fast Fourier Transform (FFT) since the data time-series is discrete and the duration T is not infinite. When $m = n$, the $G_{mn}(f)$ is named as "auto-spectra". If we are dealing with surface elevation signals $P_m(f)$, then the auto-spectra $G_{mm}(f)$ is actually an estimated variance spectrum $E(f)$. If $m \neq n$ then $G_{mn}(f)$ is indeed cross-spectra. The real part of this cross-spectra is called "coincident spectral density functions" or "co-spectra" and noted as $C_{mn}(f)$, while the "quadrature spectral density functions" or "quad-spectra" $Q_{mn}(f)$ denotes the imaginary part of $G_{mn}(f)$. One can find that the calculation of cross-spectra may be done for $m \leq n$ since $G_{mn}(f)$ is a complex conjugate of $G_{nm}(f)$.

Since earlier we applied the linear wave theory and random-phase model, the following relation holds between the cross-spectra $G_{mn}(f)$ and the directional wave spectrum $S(f,\theta)$:

$$G_{mn}(f) = \int_0^{2\pi} H_m(f,\theta) H_n^*(f,\theta) \, \mathrm{e}^{-i\boldsymbol{k}\cdot(\boldsymbol{x_n}-\boldsymbol{x_m})} S(f,\theta) \, \mathrm{d}\theta \tag{2.12}$$

Note that m = 1,...,N, and m < n. The equation above can be also expressed with the directional spreading function $D(f,\theta)$.

$$G_{mn}(f) = E(f) \int_0^{2\pi} H_m(f,\theta) H_n^*(f,\theta) \, \mathrm{e}^{-i\boldsymbol{k}\cdot(\boldsymbol{x_n}-\boldsymbol{x_m})} D(f,\theta) \, \mathrm{d}\theta \tag{2.13}$$

$H_m(f,\theta)$ is the transfer function between water surface elevation signal and other types of signals P_n, e.g., velocities, pressure, etc. The "*" sign means the complex conjugate, so $H_n^*(f,\theta)$ and $H_n(f,\theta)$ are conjugate complex quantities. Furthermore, the transfer function $H_m(f,\theta)$ can be decomposed as such:

$$H_m(f,\theta) = h_m(f) \cdot \cos^{\alpha_m}\theta \cdot \sin^{\beta_m}\theta \tag{2.14}$$

Here, different types of wave signals lead to different values of $h_m(f)$, α_m and β_m. The readers are thus referred to Benoit et al. (1997) for an elaborate table of transfer functions for various kinds of wave signals.

Equation 2.12 or 2.13 is the foundation of the conventional reconstruction methods. The directional spectra can then be estimated from the cross-spectra of the relevant wave signals. Ideally, the estimated directional spreading function is unique if an infinite number of wave signals are recorded simultaneously. However, this is not the case in reality. For most single-point measuring devices, only three wave signals are available, which gives limited information on the wave field. Assumptions must be made to get a unique solution of the DSF. Five independent quantities should be computed to estimate the variance spectrum $E(f)$ and the directional spreading function $D(f,\theta)$. These quantities can be noted as Fourier coefficients of the DSF:

$$a_n = \int_0^{2\pi} D(f,\theta)\cos(n\theta)\,\mathrm{d}\theta \tag{2.15}$$

$$b_n = \int_0^{2\pi} D(f,\theta)\sin(n\theta)\,\mathrm{d}\theta \tag{2.16}$$

For a single-point system, it is possible to use four Fourier coefficients to include all the available information on the DSF, i.e., a_1, b_1, a_2 and b_2. In Benoit et al. (1997), the expressions for these coefficients are summarized for different single-point systems.

2.4 Review of Existing Reconstruction Methods

2.4.1 Open Ocean Wave Fields

Many methods for directional wave spectra reconstruction have been developed from the 20^{th} century. An extensive review of multi-directional wave spectra reconstruction methods was given in Benoit et al. (1997), where they commented on the methods used for single-point systems and wave gauge arrays. Stochastic methods seem to be more preferred compared to deterministic techniques. For a single-point system, the Iterative Maximum Likelihood method (IMLM), the Bayesian Direction Method (BDM) and the Maximum Entropy Principle (MEP) performed accurately, these methods were found to be reasonably accurate in Benoit and Goasguen (1999), where various reconstruction methods were tested using field data, collected along the French coast, the water depth is 32 or 38m. Moderate sea conditions were observed with significant wave heights ranging from 3.5m to 4.0m.

Isobe and Kondo (1985) designed an extension of the MLM (known as EMLM) to process various types of wave properties. This method is fast and performs exceptionally well with narrow unimodal spectra. However, EMLM is highly sensitive to errors, which are made from the calculation of the cross-spectra, thus negatively affecting its reliability. Pawka (1983) proposed an iterative version of the MLM, noted as IMLM, which improved the performance of the original MLM reconstruction. The IMLM was then used to study island shadows in directional wave spectra, it was compared with the original MLM using field data for various wave conditions, the data was collected from the Southern California borderland region. 9.6m water depth was concerned. The IMLM was able to provide a higher resolution than the MLM, but it is dependent on the quality of the initial solution and can overestimate the peak in the directional wave spectra.

The Bayesian Direction Method (BDM) was suggested by Hashimoto and Kobune (1987). It does not assume a directional spreading function shape as a priori, making this method more flexible for multi-model wave spectra. Though it is complicated to implement and time-consuming in spectra reconstruction, it is still considered one of the most potent methods. However, when using a single-point system with three wave signals, the accuracy of the BDM seems to be lower compared to the situation when it is used for multi-component arrays.

Hashimoto et al. (1994) developed an extension of the MEP, which is known as the EMEP. Unlike the MEP, the EMEP can handle more kinds of measuring devices than three-quantity measurements only. It has got the advantages of the BDM, and with a faster computational speed. The high tolerance to errors of the EMEP is also an advantage when applying this method to real-world data. The EMEP was then compared with the BDM, EMLM in Hashimoto (1997) using field data from the Iwaki Offshore Station. The significant wave height was 3.81m and the significant wave period was 12.3s. It was found that the EMLM showed a much lower directional peak than the other two methods, while the EMEP and the BDM provided more concentrated estimates around the peak.

Among the existing literature, perhaps the most commonly used methods nowadays are MEP, MLM, the Bayesian Direction Method (BDM), and various extended or modified versions of these methods.

2.4.2 Reflective Wave Fields

In the existing literature, most methods for estimating the multi-directional wave spectra assume open ocean conditions. However, reflection can also be crucial in the coastal zone. Numerous methods have been developed in this regard. Here we introduce several representative methods working on the directional spectra estimation in reflective wave fields, the gauge arrays are applied in these methods.

Isobe and Kondo (1985) developed an adjusted MLM method, usually referred to as the modified maximum likelihood method (MMLM), for calculating wave spectra with strong phase-locked reflective waves. Later, Hashimoto and Kobune (1987) proposed a modified Bayesian method that is capable of doing a similar job. However, both of them require the position of the reflection line as one of the input parameters, while this reflection line is difficult to determine in the real world.

Davidson et al. (1998) proposed an advanced method based on Isobe and Kondo (1985). Instead of a necessary input, the reflection line is determined with an iteration process. This method has shown good capability in the test using both field and artificial data, as long as the measuring probes are close to the reflector. However, if the probes are located further offshore, this method may produce spurious peaks in the directional spectra.

Recently, Draycott et al. (2016) developed a new technique named Single-summation PTPD Approach with In-line Reflections (SPAIR) method. The PTPD approach assumes that the reflective waves mirror the incident waves. A series of lab experiments have proved that the SPAIR method could produce improved estimations of directional wave spectra compared to the commonly used methods. The incident and reflected wave spectra can be distinguished in the time and frequency domain over all the directions; however, if the reflective waves are oblique to the incident waves (especially when the angle is higher than 20°), the method cannot separate them anymore. The presence of oblique reflective waves indicates the necessity for further improvement of this method.

These methods are still limited, more testing and investigation are needed.

2.4.3 Directional Wave Spectra Reconstruction of IG Waves

We have shown known that all the available reconstruction methods assume the linear wave theory, while non-linear interaction of two wave components generates a forced IG wave component. The linear dispersion relationship does not hold for these waves, thus bound and free waves with the same frequency can have different velocities, c_{bound} and c_{free}. In other words, the presence of bound IG waves would "contaminate" the measured data, leading to less accurate directional spectra reconstructions.

The velocity difference of bound and free IFG waves is small in very shallow waters (Brillouin, 1960), making using existing 2D spectra reconstruction methods possible. See Figure 2.1 for an example. van Essen et al. (2013) compared three methods for IG wave fields (two cases were considered: bound waves only; bound and free waves) and predicted the motion response of liquid natural gas (LNG) carriers in nearshore areas with water depths ranging from 15m to 40m. Two stochastic methods, the EMEP and the BDM, and a deterministic method named

r-DPRA (de Jong and Borsboom, 2012), were compared in this paper.

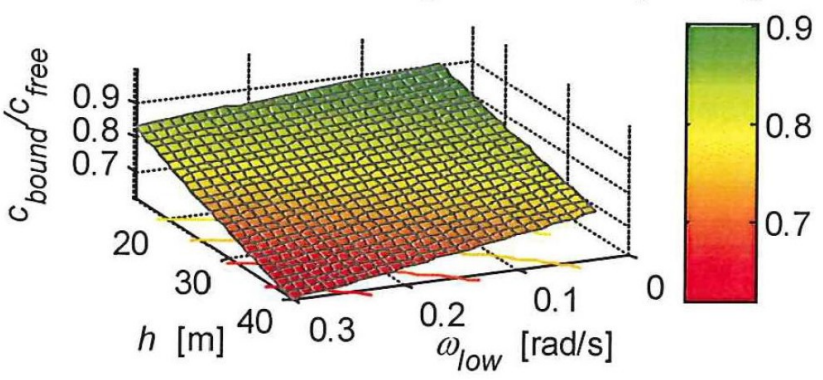

Figure 2.1: Velocity ratio of 1D bound and free IG waves. (van Essen et al., 2013)

Although assuming free waves, the presented methods still did fine for shallow water and narrow DSF. The errors due to the linear wave assumption are evenly distributed over all directions on the reconstructed directional wave spectra, and these errors increase quadratically with higher water depths. When considering bound and free IG wave components, it turned out that r-DPRA is incapable of finding the corresponding waves, and the BDM could not find the secondary incident peak. The EMEP, on the other hand, provides reasonable estimation for all tested conditions. Higher input error tolerance might be one of the reasons that the EMEP outperforms the other two methods. The comments to these methods are based on several parameters, including the root-mean-square wave height H_{rms}, the mean wave period T_{mean}, the dominant direction θ_{dom} and the spectral width σ_s, whereas these parameters are derived from the full spectra with IG and SS frequency ranges. However, the IG energy, compared to the SS energy, is relatively weak and thus does not significantly influence these parameters. Moreover, the detailed situation of reconstructed spectra at IG frequencies is not clearly shown in this paper. Also, note that the distinction of bound and free IG waves is not possible since all the methods used here use linear wave assumption. The problems mentioned above motivate new work to investigate the detailed situation at IG frequencies. The detailed situation of the reconstructed spectra at different IG frequencies should be investigated for different reconstruction methods, in order to get a better understanding of the reliability of these methods.

2.4.4 REFLEX Measurement Campaign

From mid-November 2021, a series of large-scale field experiments have been conducted at the sand engine, the Netherlands. The work serves as part of the REFLEX (Infragravity wave REFlection and dune erosion during EXtreme Storms) project. These experiments aim to investigate the hydrodynamics during wave attacks in the coastal dune area. It is well known that the short waves tend to break or dissipate in the shallow coastal area, while IG waves will not

lose much energy when approaching the coastal dunes (Herbers et al., 1994). This mechanism may lead to the dominant role of the IG wave in the dune erosion process (Lashley et al., 2019). Therefore, one of the critical points of this project is to assess the contribution of the IG wave field to the dune erosion.

This report aims to fit itself into the REFLEX project, providing references on 2D directional wave spectra reconstruction in the coastal wave field with IG waves. The considered water depth is well below 15m, which motivates the continuation of work done by van Essen et al. (2013). Artificial data will be generated in such a way as to mimic the actual conditions. The performance of the chosen wave spectra estimation methods will be checked using these data. Here, IMLM, BDM and EMEP are selected. A general introduction to these methods will be given later. For elaborated introductions, please see Benoit et al. (1997) and Hashimoto (1997).

2.5 Research Objectives and Research Questions

To examine the performance of the wave spectra reconstruction method on the IG wave field, a general research objective, as well as several specific research questions, are formulated below.

Research goal: Compare several commonly used wave spectra reconstruction methods and examine their performances on SS and IG wave fields.

Research questions:

- What are the commonly used methods in the existing literature?
- How to generate artificial data?
- What are the influences of bound IG waves in wave spectra reconstruction?
- How do the selected methods perform? Is there a "best" method that consistently produces better results than other methods do, or these methods have their advantages in different conditions?

3 Methodology

3.1 Introduction

The general approach of this research was to generate artificial wave signals using pre-defined directional wave spectra, different types of wave signals, i.e., surface elevation, velocities, pressure, were produced and processed. These wave signals were analyzed using different wave spectra reconstruction methods. The outputs are then the estimated wave spectra for the interested wave conditions. In the REFLEX project, Acoustic Doppler Current Profilers (ADCP) were used in the field for hydrodynamical measurements. Surface elevation, two orthogonal velocity components at assigned depths, pressure signals measured from the bottom of the devices were obtained from those ADCPs. These wave signals were generated from the predefined 2D wave spectra to imitate the features of the field measurements. Two representative measurement spots were selected: the water depths at these devices are 14m and 8m, respectively. The significant wave height H_s at these locations varies from 1m to 4m and the peak wave period $T_p$ranges from 4s to 10s.

Three reference tests were arranged to represent different wave conditions. First, we only concentrate on the spectra estimation for the SS frequency domain. Then free IG waves and bound IG waves were added to the analysis, respectively. Three selected methods, as introduced in chapter 2, were applied and compared.

3.2 Data Preparation

A set of MATLAB codes were used to generate the artificial wave field from the user-defined 2D wave spectrum. The considered frequency range was 0.04-0.3 Hz for SS waves and 0.005-0.04 Hz for IG waves. The frequency resolution was 0.0002 Hz, and the directional resolution was 5°. The free IG waves and the bound IG waves, could be generated separately.

The 2D JONSWAP spectra were used to generate wave data series at SS frequencies. The significant wave height, peak wave period, peak direction of the SS waves, and the directional spreading parameter for cos-2s modal should be included to define the 2D directional spectrum.

A commonly used model for describing the shape of the directional energy distribution is the $\cos^{2s}$ model:

$$D(\theta) = A\cos^{2s}\left[(\theta - \theta_0)/2\right] \tag{3.1}$$

θ_0 indicates the mean wave direction and s a factor influencing the spectral width of $D(\theta)$. A represents a normalization constant. The spectral width σ is defined as the standard deviation of the dominant direction, and it can be related to the controlling factor s in the following way (Kuik et al., 1988):

$$\sigma = \left(\frac{2}{s+1}\right)^{1/2} \tag{3.2}$$

Theoretically, the maximum value of σ is 81.03°. The spectrum for free IG waves is described in Ardhuin et al. (2014), the empirical parameterized equations of the IG waves are given below:

$$A_{IG} = H_s T_{m0,-2}^2 \tag{3.3}$$

$$E_{IG}(f) = 1.2\alpha_1^2 \frac{kg^2}{C_g 2f\pi} \frac{(A_{IG}/4)^2}{\Delta f}\left[\min(1, 0.015Hz/f)\right]^{1.5} \tag{3.4}$$

In which, α_1 is dimensional tuning parameter, we set $\alpha_1 = 10 \times 10^{-4} s^{-1}$.

The mean wave period is determined by moments $T_{m0,-2} = \sqrt{m_{-2}/m_0}$, where the n-th order moment is defined as:

$$m_n = \int_{0.04Hz}^{0.3Hz} E(f) f^n \, \mathrm{d}f \tag{3.5}$$

The spectrum for bound IG waves can be produced following Hasselmann (1962), the equation to calculate the bound IG wave spectra $E_{forced}(\Delta f)$ is given below:

$$E_{forced}(\Delta f) = 2\int_{\Delta f}^{\infty} \mathrm{d}f \int_0^{2\pi} \mathrm{d}\theta_2 D^2(f + \Delta f, -f, \Delta\theta + \pi) E(f + \Delta f, \theta_1) E(f, \theta_2) \tag{3.6}$$

Here, $E(f, \theta)$ is the SS wave energy density directional spectrum. $D(f + \Delta f, -f, \Delta\theta + \pi)$ is the difference-interaction coefficient for two waves with frequencies f and $f + \Delta f$ and directional differences $\Delta\theta (= |\theta_1 - \theta_2|)$.

The relative contribution of bound IG waves was measured using a squared ratio R^2, similar to equation (9) in Reniers et al. (2021).

$$R^2_{bound} = \frac{H^2_{m0,bound}}{H^2_{m0,bound} + H^2_{m0,free}} \tag{3.7}$$

In this study, the sampling rate of the measurements was 4 Hz, which is the same as applied in the field. Since artificial data was used, numbers of segments of data series were produced and connected to a long record to improve estimate quality. The length of each segment represents approximately 15 minutes, hence 4096 data points were produced for each segment. Linear interpolation was used to connect these signals, i.e., ten NANs were added between each segment, then we replaced them by linear interpolation, ensuring the wave signals are smooth.

The reason that this connection was adopted for the pre-processing is to mimic a Gaussian wave field. When generating synthetic data, we must indicate an initial phase to the wave components, as shown in equation 2.6. However, since the frequency domain is not continuous, the phase difference between two wave components is fixed, while the phase difference is random for a Gaussian wave field. Therefore, more than one artificial record is needed to simulate the actual condition and reduce the errors from the cross-spectral calculation.

Gaussian white noise were added into the time series, the noise level is expressed by the variance of the data, i.e., $noise\ level \cdot var(data)$. In this way, the artificial data can be more similar to the real-world measurement outputs. Unless specifically mentioned, the noise level is 0.2 for the numerical tests. Moreover, if not specified, the location of the velocity measurements is 0.5m to the water surface, the directional width σ is 20$\circ$.

The table below summarizes the tests with only SS waves. Note that the case 1 to case 3 are the reference tests.

Case	Significant wave height [m]	Peak period [s]	Water Depth [m]	Directional width [$\circ$]
1	2	6	14	20
2	3.25	8	14	20
3	4	10	14	20
4	3.25	8	14	10
5	3.25	8	14	30
6	2.5	6	8	20
7	4	6	14	20

Table 3.1: Overview of tests with SS waves.

Case	Considered Parameter	Range
1	Noise level	0-1.2
2	Velocity measurement location	1.5m-13.5m
3	Significant wave height	2m-4m
4	Peak period	6s-10s
5	Spreading factor	10-35

Table 3.2: Overview of the sensitivity tests.

Case	Significant wave height [m]	Peak period [s]	Water depth [m]	Noise level	Mean direction of incident free IG waves [$\circ$]
1	3.25	8	14	0.2	0
2	2	8	14	0	0
3	4	8	14	0	0
4	4	8	8	0	0
5	3.25	8	14	0	15
6	3.25	8	14	0	45

Table 3.3: Overview of tests with IG waves

A series of sensitivity tests are summarized in Table 3.2, only SS waves included. Moderate wave condition was used, $H_s = 3.25m, T_p = 8s$, water depth = 14m. A number of test cases with SS and IG waves are summarized in 3.3.

3.3 DIWASP

3.3.1 Working Procedure

An open-source directional wave spectra analysis toolbox, DIWASP, was used in this study. (Johnson, 2002) DIWASP is a MATLAB toolbox for the estimation and analysis of directional spectra. The source code, as well as the manual, can be found at GitHub (https://github.com/metocean/diwasp). The artificial data time-series obtained from the mentioned wave generation program serve as the input of this toolbox. Three data structures needed to be specified before the wave spectra estimation.

- The instrument data. (**ID**) The layout of the instrument, the data types and the data time series should be specified. Considered water depth and sampling frequency must be pointed out in **ID**.
- The spectral matrix. (**SM**) This structure will contain the estimated spectra as outputs. The orientation of the axes system and the frequency/direction range must be included before the estimation process begin.
- The estimation parameters. (**EP**) In this structure, the wave spectra reconstruction method needed to be chosen. Several method-related parameters can be modified, more detailed information can be found in the DIWASP manual.

After specifying the required information, one can start the analyzing process by simply calling the "dirspec" function. The cross-spectra are computed by "csd" function, where the window size was set to 1024 with 256 data points overlapping. The "plotspec" function can give the user some first visualizations of the outputs, polar plots and 3D surface plots may be chosen.

Plant and Donelan (2020) suggested a way to measure the difference between the original wave spectrum and the reconstructed one, which was adopted for this study:

$$\%Error \ = 200 \times \frac{\sum_\theta |D(Input) - D(recovered)|}{\sum_\theta [D(Input) + D(recovered)]} \tag{3.8}$$

A flow chart is given below to illustrate the process of analyzing work:

3.3.2 Reconstruction Methods

In this study, 2D wave directional analysis is conducted using three conventional wave spectra reconstruction methods: EMEP, BDM, and IMLM. These methods were selected from the DIWASP toolbox, here we give some general introduction.

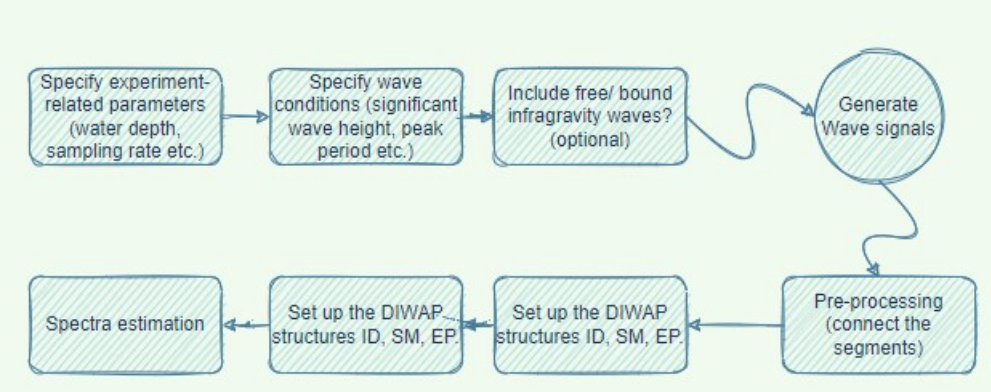

Figure 3.1: Flow chart showing the working process

IMLM

The IMLM is chosen since it is an efficient refinement of the popular MLM. For the MLM, the idea is that the directional spreading function can be noted as a linear combination of the cross-spectra. The estimation of the DSF is:

$$\hat{D}_{MLM}(f,\theta) = \frac{1}{\hat{E}(f)} \sum_{m,n} \alpha_{mn}(f,\theta) \cdot G_{mn}(f) \tag{3.9}$$

$\hat{D}_{MLM}(f,\theta)$ is the estimated DSF, and $\hat{E}(f)$ indicates the reconstructed variance spectrum.

An estimate that has been proven best is found:

$$\hat{D}_{MLM}(f,\theta) = \frac{\kappa}{\sum_{m,n} H_m(f,\theta) G^{-1}_{mn}(f) H^*_n(f,\theta)} \tag{3.10}$$

$G^{-1}_{mn}(f)$ implies the elements of the inverse of the cross-spectral matrix, κ is a parameter determined based on equation 2.5. However, computed cross-spectra from the MLM is not consistent with the cross-spectra calculated from the wave signals. Iterative refinement is then introduced by Pawka (1983). The IMLM follows the expressions below:

$$\hat{D}^i_{IMLM}(f,\theta) = \hat{D}^{i-1}_{IMLM}(f,\theta) + \varepsilon^i(f,\theta) \quad and \quad \hat{D}^0_{IMLM}(f,\theta) = \hat{D}^0_{MLM}(f,\theta) \tag{3.11}$$

$$\varepsilon^i(f,\theta) = \frac{|\lambda|^{\beta+1}}{\lambda\gamma} \quad with \quad \lambda = \hat{D}_{MLM}(f,\theta) - \Delta^{i-1}_{MLM}(f,\theta) \tag{3.12}$$

In which, Δ^{i-1}_{MLM} indicates the MLM estimate based on $\hat{D}^{i-1}_{IMLM}(f,\theta)$. β and γ influence the

convergence of the IMLM algorithm, typically of order 10 for γ and of order 1 for β. The iterative process stops after a number of steps or when the convergence is satisfied. In this way, the IMLM significantly improves the MLM estimation.

BDM

The BDM method is originated from the Bayesian technique applied in probability theory. Although hard to implement and not advised for single-point systems, it is still a powerful method since no priori of the shape of the DSF is formulated. The BDM divides the range 0-2π to many segments K, the width is then $\Delta\theta = 2\pi/K$. The estimated directional spreading function is regarded as constant for each segment. We have:

$$X_K = \ln[\hat{D}_{BDM}(\theta_k)], \quad \theta_k = (k - 1/2)\Delta\theta \tag{3.13}$$

$$\hat{D}_{BDM}(\theta) = \sum_{k=1}^{K} \exp(x_k) \cdot I_k(\theta) \tag{3.14}$$

Here, $I_k(\theta)$ is 1 if $(k-1)\Delta\theta \leq \theta \leq k\Delta\theta$, $I_k(\theta)$ is 0 for other situations. K is often in the order of 40-90, which indicates a high degree of freedom. In other words, the unknowns are far more than the number of equations derived from the cross-spectra. This feature of the BDM leads to its ability to detect most of the DSF shapes. The smoothness of the DSF and errors in the cross-spectra estimation are also taken into account.

EMEP

Since recommended by van Essen et al. (2013), the EMEP is also selected. The EMEP is an improvement of the original MEP method. For the MEP, the idea is based on the Shannon definition of entropy. The entropy H is defined as:

$$H(\hat{D}) = -\int_0^{2\pi} \hat{D}(\theta) \ln(\hat{D}(\theta))\, \mathrm{d}\theta \tag{3.15}$$

Based on the MEP estimate, the EMEP estimate takes the following form:

$$\hat{D}_{EMEP}(f,\theta) = \frac{1}{\Delta} \exp \sum_{k=1}^{K} [A_k \cdot \cos(k\theta) + B_k \cdot \sin(k\theta)] \tag{3.16}$$

with

$$\Delta = \int_0^{2\pi} \exp \sum_{k=1}^{K} [A_k \cdot \cos(k\theta) + B_k \cdot \sin(k\theta)] \, \mathrm{d}\theta \tag{3.17}$$

A_k and B_k ($k = 1,\ldots,K$) are unknown values. The EMEP is better than the MEP since the number of harmonics in the above estimates is adapted to the cross-spectral information. Although the EMEP produces the same estimates as the MEP for single-point systems, we still use this method as a potent candidate for this study.

4 Results

4.1 Analyzed Results of SS Waves

In this section, the analyzed results of the benchmark tests will be described first. Then several sensitivity tests regarding the noise level and other parameters are given. Some special issues of the BDM are discussed in the end.

4.1.1 Benchmark Tests

Figure 4.1 shows the analyzed results for wave condition $H_s = 2.5m, T_p = 6s$ at 14m water depth, the original directional wave spectrum is given in (a). Unless specified, the direction width of the spectrum is always 20°. The reconstructed spectra from the three selected methods are demonstrated in (b), (c), and (d), respectively. It can be observed that the reconstruction methods can produce the correct shape of the direction spectrum. The mean direction and the peak frequency can be detected accurately as well. However, compared to the original spectrum, the reconstructed ones are less smooth.

The 3D surface plot as given in figure 4.1 may serve as a direct impression of the estimates. A more precise interpretation of the results is to use polar plots, as shown in figure 4.2. The methods produce the spectra differently, which is not easy to distinguish the differences using 3D surface plots, for example, the EMEP gives a slightly larger estimate at higher frequencies than the other methods in this test.

Then, we gradually increase the wave height and the peak period, as shown in figure 4.3 and figure 4.4. The water depth is kept as 14m; actually, these estimates do not change much if we use 8m water depth instead. Again, the mean direction and the peak period of the wave field can be detected by these methods well. However, the BDM fails around the peak frequency. This failure can be encountered in various conditions, and we will discuss this phenomenon later.

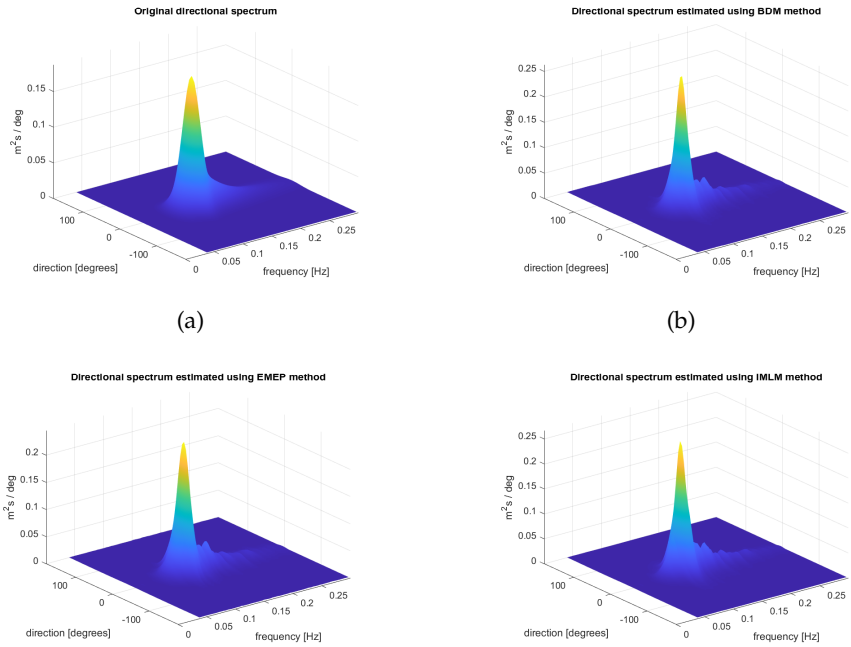

(a) (b)

(c) (d)

Figure 4.1: Analyzed results for $H_s = 2.5m, T_p = 6s$, water depth = 14m, compared with the original spectrum (3D visualization).

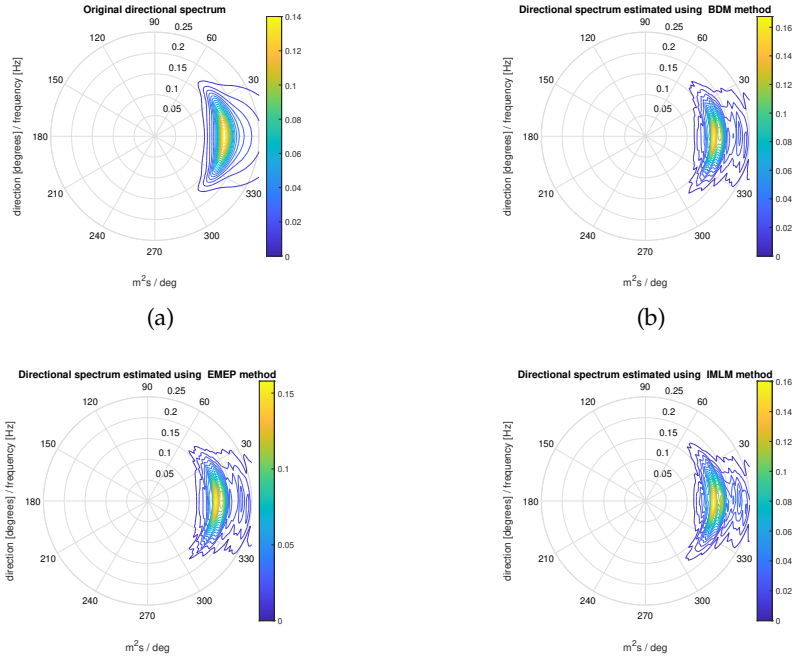

(a) (b)

(c) (d)

Figure 4.2: Analyzed results for $H_s = 2.5m, T_p = 6s$, water depth = 14m, compared with the original spectrum.

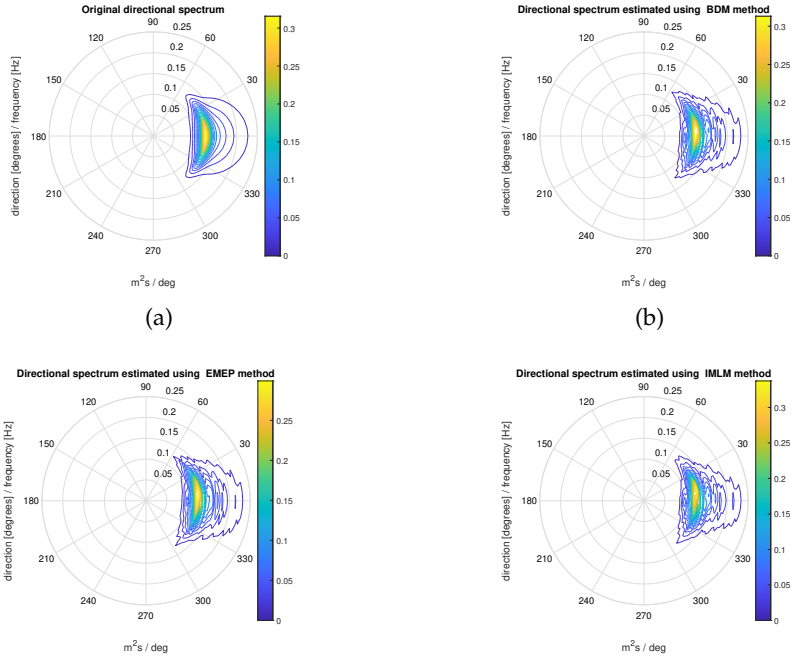

(a) (b) (c) (d)

Figure 4.3: Analyzed results for $H_s = 3.25m, T_p = 8s$, water depth = 14m, compared with the original spectrum.

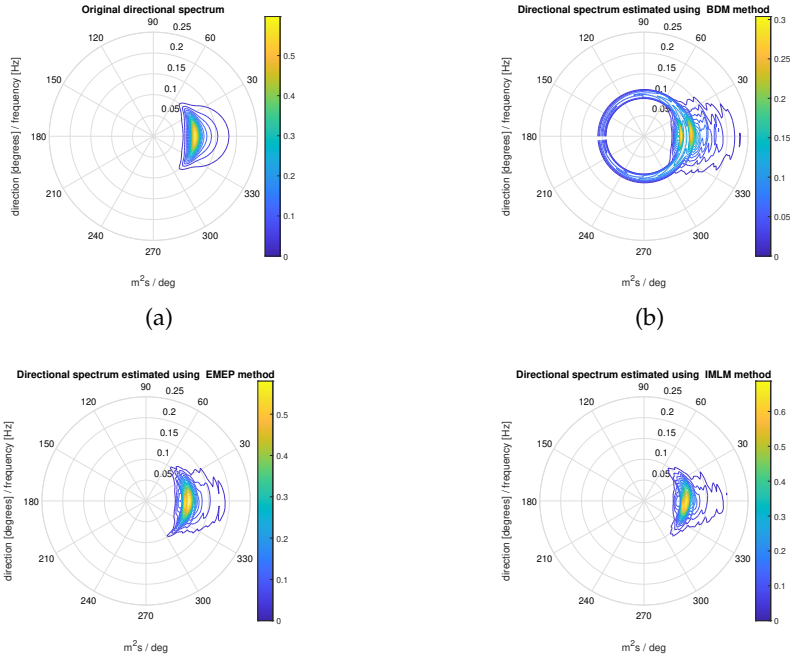

(a) (b) (c) (d)

Figure 4.4: Analyzed results for $H_s = 4m, T_p = 10s$, water depth = 14m, compared with the original spectrum.

4.1.2 Sensitivity Tests

Noise Level

Several sensitivity tests are conducted to show how the methods react to the change of a particular parameter. Figure 4.5 illustrates the percentage error of the reconstructed spectra performed by different methods when changing the white noise level. For this case, $H_s = 3.25m, T_p = 8s$, which can be regarded as a moderate wave condition. The IMLM seems to be the most sensitive to the noise, the % error ranges from approximately 14% to 32.5%, while the EMEP is more robust than the other methods, the % error varies from around 6% to 17.5%.

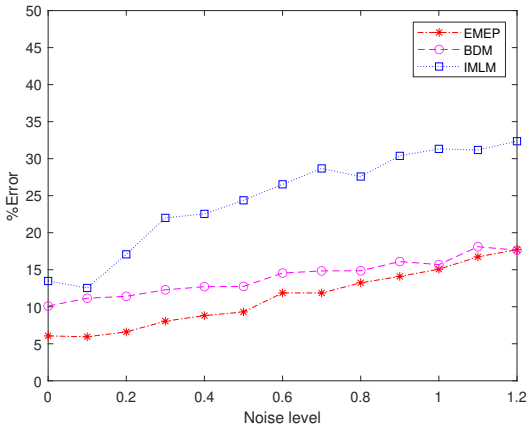

Figure 4.5: %Error when changing noise level. $H_s = 3.25m, T_p = 8s$, water depth = 14m, for EMEP (red), BDM (magenta) and IMLM (blue).

Location of the Velocity Measurement

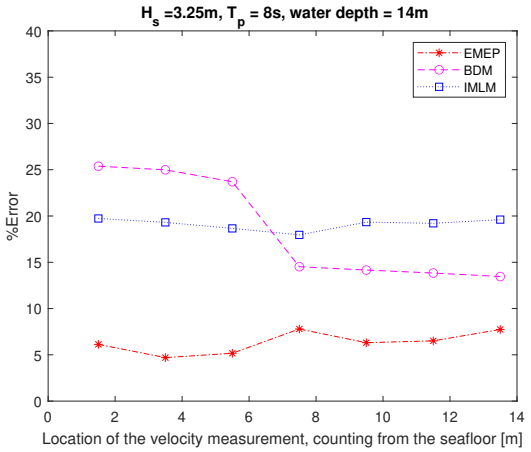

Figure 4.6: %Error when changing location of the velocity measurement, counted from the sea floor. $H_s = 3.25m, T_p = 8s$, water depth = 14m, for EMEP (red), BDM (magenta) and IMLM (blue).

The location of the velocity measurement can be varied for the ADCPs, here we change it from 1.5m to 13.5, counting from the seafloor. Figure 4.6 gives an example of this, it is clear that the EMEP and the IMLM are not sensitive to the location of the velocity measurement, while the BDM does yield finer estimates if the velocity measurement is closer to the water surface. The EMEP always produces better estimates compared to the other methods.

Wave Height and Wave Period

If we keep the wave height the same and change the wave period or vice versa, the quality of the estimates may be influenced. Figure 4.7 provides an example. If wave height is too high, the BDM will fail severely, while the other two methods are not significantly affected. The IMLM seems not stable when changing peak period, while the other two methods are stable. Generally, the EMEP performs best in these conditions. The BDM often provides a fairly good estimate unless the high wave height. The IMLM is the least accurate method, as shown here; however, it will never fail around the peak frequency.

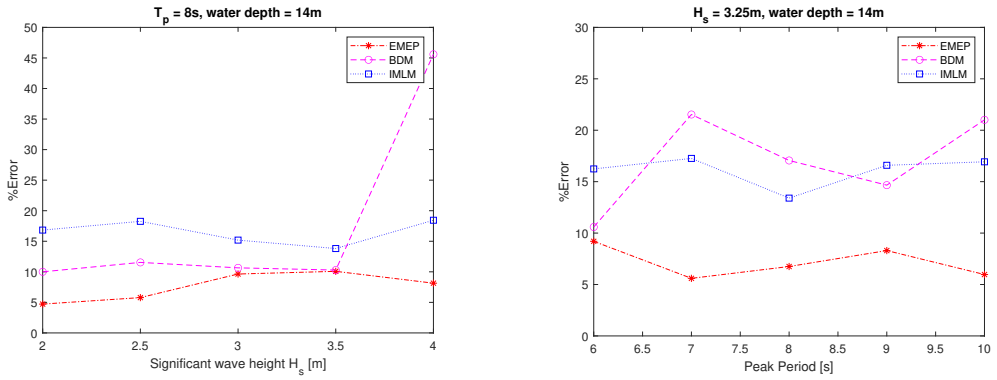

(a) (b)

Figure 4.7: %Error when changing significant wave height or peak period, water depth = 14m, (a): keep $T_p = 8s$, change significant wave height H_s; (b): keep $H_s = 3.25m$, change significant wave height T_p, for EMEP (red), BDM (magenta) and IMLM (blue).

Spreading factor

The spectral width σ is varied to test the sensitivity of these methods on the broadness of the wave. Figure 4.8 (a) gives a graphical explanation of the relation between the direction width and the spreading factor; note that in the wave generating program, we have to modify s instead of σ. From figure 4.8 (b). The BDM would not be reliable anymore if the spectrum were too narrow, while the EMEP and the IMLM are not sensitive to the direction width of the target spectrum. The EMEP provides quite accurate results no matter how the σ is changed.

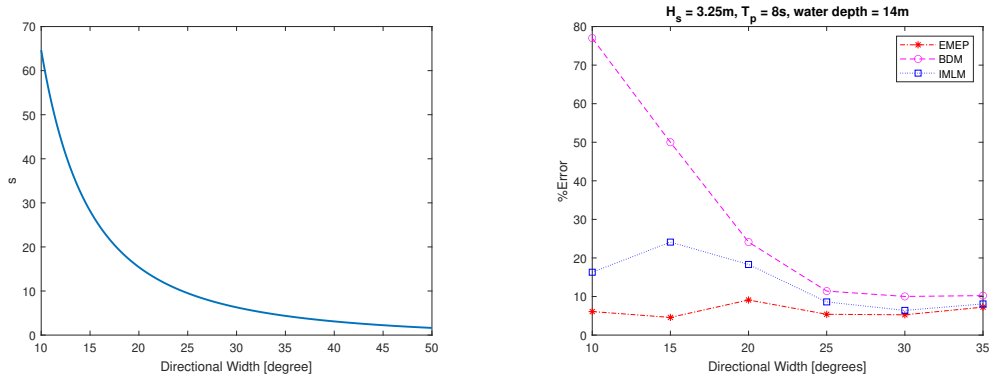

(a) (b)

Figure 4.8: (a): The relation between the directional width σ and the spreading factor in $\cos^{2s}$ model; (b): %Error when changing spreading factor s, $H_s = 3.25m, T_p = 8s$, water depth = 14m, for EMEP (red), BDM (magenta) and IMLM (blue).

4.1.3 Special Issues Regarding the BDM

Usually, the BDM can produce reliable estimates, but it may fail in some conditions, as shown in the previous sections. The phenomenon is that the reconstructed spectrum would not provide the correct shape around the peak frequency. For example, Figure 4.4 clearly shows the reconstructed spectrum around the peak frequency is wrong and evenly distributed over all directions. This problem will occur if the BDM is dealing with a narrow spectrum, see figure 4.8 (b).

Figure 4.9 compares the analyzed results from the BDM for the same wave conditions with different spreading factors. The BDM provides a nice estimation for the $\sigma = 30°$ case. For the $\sigma = 10°$ case, though the estimation looks fine at other frequencies, the spectrum is nearly evenly distributed around the peak frequency. The BDM is hence not acceptable in this case.

Figure 4.10 illustrates the detailed situation of the DSF at the peak frequency, for this particular case, $f = f_p = 0.125Hz$. For the narrow spectrum case (a), it is indeed true that the BDM estimate yields an evenly distributed spreading function over the directional domain. In this case, this failure of the BDM would not happen for a broad target spectrum.

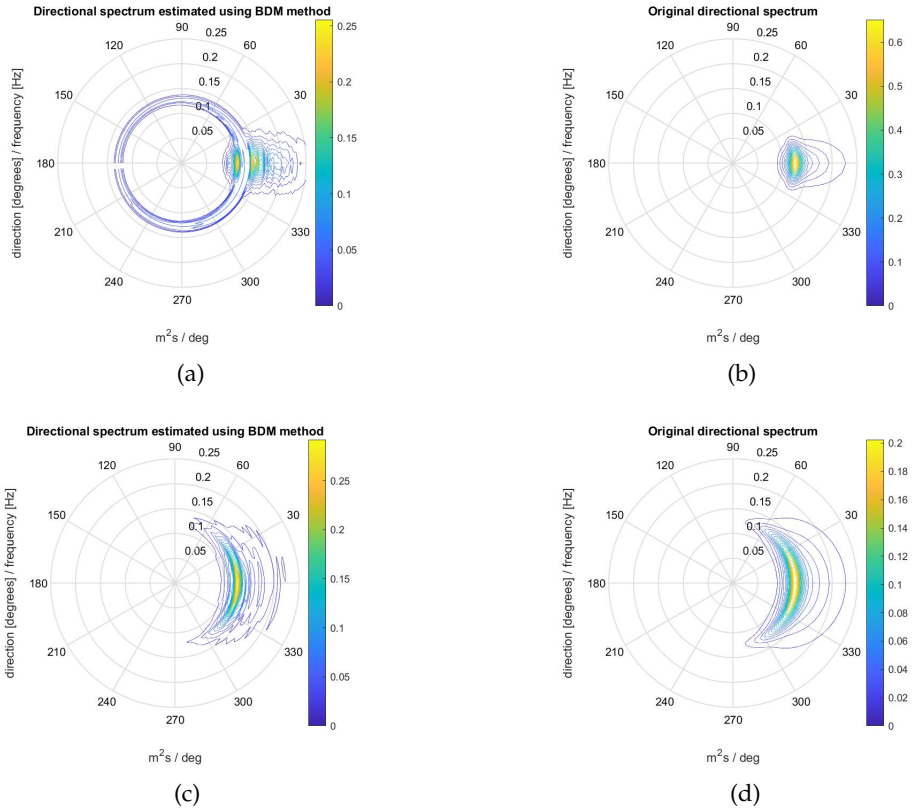

Figure 4.9: Analyzed results from the BDM, compared with the original spectrum, $H_s = 3.25m, T_p = 8s$, water depth = 14m. (a), (b): $\sigma = 10°$; (c), (d): $\sigma = 30°$, for original (dashed line), EMEP (red), BDM (yellow) and IMLM (blue).

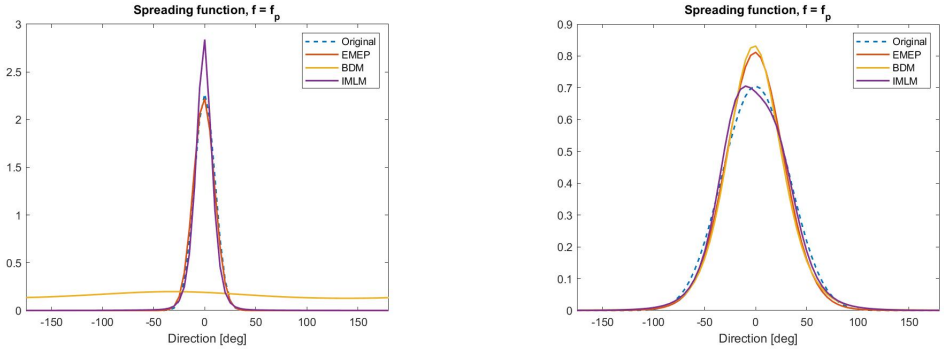

Figure 4.10: Analyzed results at the peak frequency, compared with the original spectrum, $H_s = 3.25m, T_p = 8s$, water depth = 14m. (a): $\sigma = 10°$; (b): $\sigma = 30°$, for original (dashed line), EMEP (red), BDM (yellow) and IMLM (blue).

An investigation of this problem was carried out to relate this failure to some non-dimensional parameters, for instance, wave steepness or the ratio of wave height and water depth. However, it seems that the problem does not relate to these parameters. Figure 4.11 (a) and (b) show

the analyzed results from the BDM and the original spectrum as well. The ratio wave height over water depth for this case is higher than most cases with a 14m water depth, but the BDM estimate is still accurate. Changing peak period to vary the wave steepness does not give a clue of this, for a high wave height case $H_s = 4m$, varying peak period from 6s to 10s always leads to the false directional peak at the peak frequency, see figure 4.11 (c) and (d). Figure 4.12 compared the DSF at the peak frequency for two cases shown in figure 4.11. For (b), the BDM provides a less spread estimate, compared to figure 4.10 (a). The problem seems related to the wave height, hence the wave energy of the spectrum. Moreover, the BDM can not deal with a very narrow spectrum.

Since the other two methods do not have this drawback, the problem of the BDM is not due to the errors from the cross-spectral calculation. The issue may be originated from the inherent flaw of the BDM. More investigations are needed.

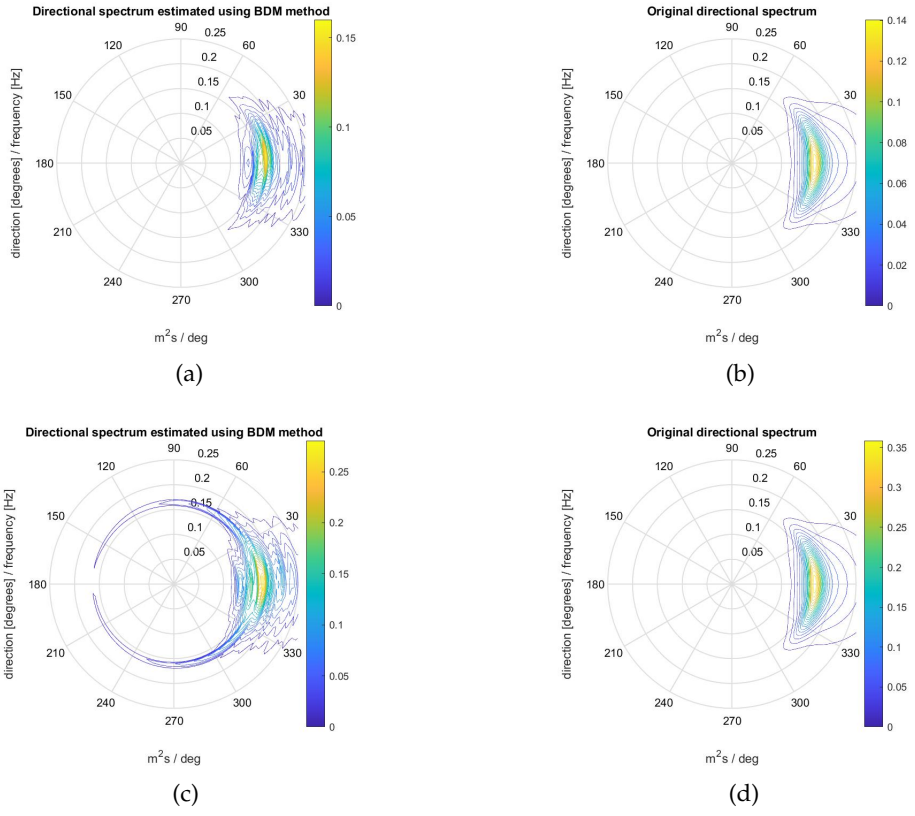

Figure 4.11: Analyzed results from the BDM, compared with the original spectrum, $\sigma = 20°$. (a), (b): $H_s = 2.5m, T_p = 6s$, water depth = 8m; (c), (d): $H_s = 4m, T_p = 6s$, water depth = 14m.

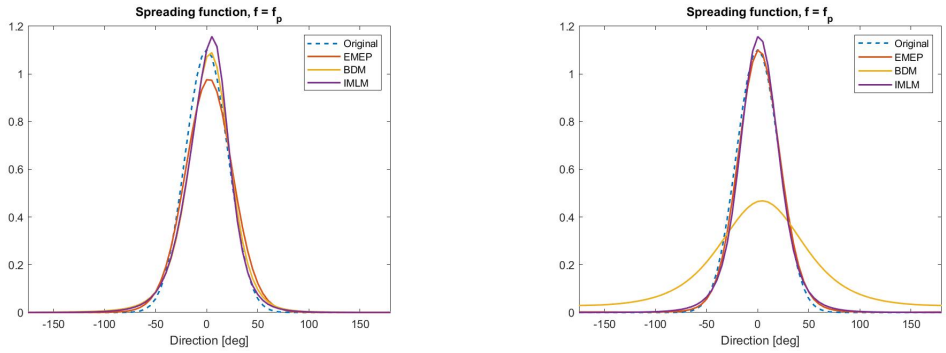

(a) (b)

Figure 4.12: Analyzed results at the peak frequency, compared with the original spectrum. (a): $H_s = 2.5m$, $T_p = 6s$, water depth = 8m; (b): $H_s = 4m$, $T_p = 6s$, water depth = 14m, for original (dashed line), EMEP (red), BDM (yellow) and IMLM (blue).

4.2 Analyzed Results of IG Waves

In this section, the free and bound IG wave signals will be added to the SS wave signals and analyzed by the selected methods. The IG spectrum is derived from the SS spectrum, and the wave energy in the IG frequency domain is much lower than that in the SS frequency domain. Therefore, it is hard to visualize the whole spectrum in one polar plot or 3D surface plot. The IG part is not visible from such a figure, and we are more interested in the detailed situation in the IG frequency range; thus, we will look closely at the reconstructed DSF in the IG frequency domain.

4.2.1 Free IG Wave Fields

Figure 4.13 demonstrates the analyzed results at different frequencies at the IG frequency range. Overall, the IMLM always gives slightly narrower estimates while the EMEP produces broader ones. The most important phenomenon observed in these figures is the energy that emerges opposite of the dominant direction at low frequencies. This false directional distribution is visible until higher frequencies, in this case, the DSF looks fine at $f = 0.1Hz$ or higher. If integrating the DSF over the IG frequencies 0.005-0.04 Hz, the false directional distribution still takes a dominant role hence cannot be neglected.

Investigations have been carried out to find the reason for this awkward estimation for IG waves. It turns out that this problem is due to the error of the cross-spectra calculation before the methods get involved. It can be shown that the white noise would provoke this problem for some reason and leads to unrealistic estimates, see figure 4.14. If we exclude the wave signals but keep the associated white noise and analyzing it using the selected methods, the white

noise is interpreted as such. Note that the original spectrum is held for reference. Since adding white noise also means adding energy to the signals, and the IG wave energy is much lower than SS energy, the reconstructed DSF is less accurate at IG frequencies. Therefore, the white noise is excluded hereafter to investigate the effect of bound IG waves.

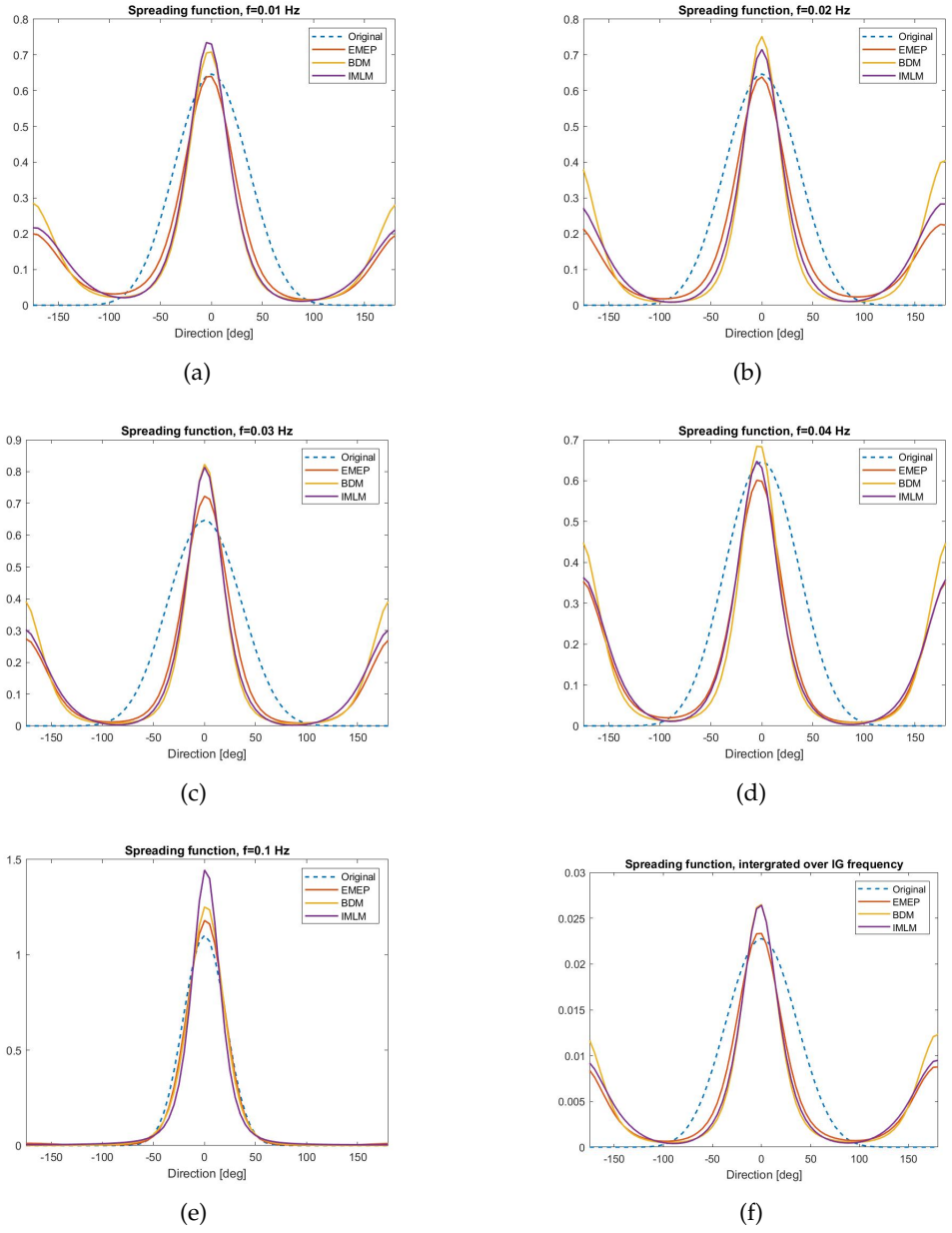

Figure 4.13: Analyzed results at different frequencies, compared with the original spectrum, $H_s = 3.25m, T_p = 8s$, water depth = 14m, bound waves are not included. (a)-(e): directional spreading function at different frequencies; (f): Directional spreading function, integrated over IG frequency range 0.005-0.04 Hz, for original (dashed line), EMEP (red), BDM (yellow) and IMLM (blue).

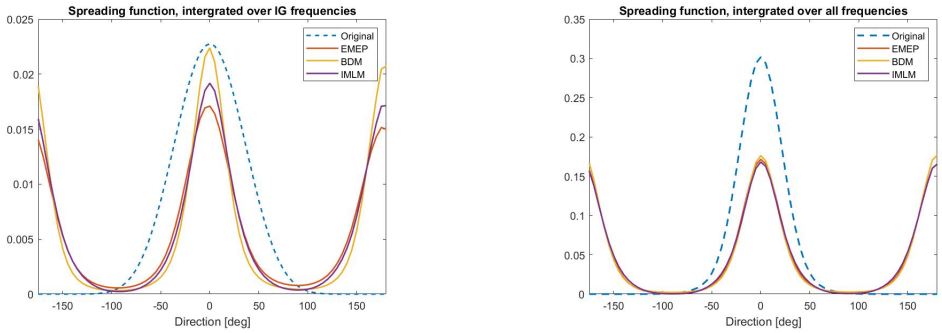

(a) (b)

Figure 4.14: Analyzed results for white noise only, same case as before, the noise level is 0.2. (a): The directional spreading function, integrated over IG frequencies; (b): The directional spreading function, integrated over all frequencies, for original (dashed line), EMEP (red), BDM (yellow) and IMLM (blue).

4.2.2 Bound IG Wave Fields

A simple way to vary The relative contribution of bound IG waves is to alter the significant sea swell wave height or the water depth, as shown in figure 4.15.

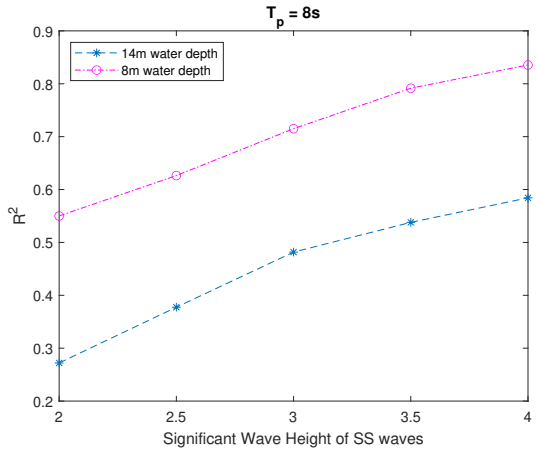

Figure 4.15: The relative contribution of bound IG waves R^2, $T_p = 8s$; star: water depth = 14m; square: water depth = 8m.

The effect of bound IG waves is demonstrated using figures in the following pages. See figure 4.16 to figure 4.18. The squared ratio R^2 is 0.2721, 0.5843, and 0.8355 for these tests, respectively. We keep the peak period of swells the same; increasing significant SS wave height or decreasing water depth results in a higher relative contribution of bound IG waves. If we neglect bound IG waves, the methods provide similar estimates. The IMLM tends to estimate the spectrum with a narrower peak, while the EMEP estimates are often broader than the IMLM.

If bound waves are also considered, please see the right panel of these figures for comparison. The estimates this time are more scattered for these methods. The IMLM yields narrower spectra, and the EMEP is broader. The BDM also gives results similar to the EMEP but closer to the original spectrum. But with increasing bound wave components, the BDM tends to produce spectra slightly spread in the opposite of the mean incident direction.

Figure 4.19 and 4.20 show the effect of bound waves when the incident direction of the free IG waves is varied. Though these methods are able to detect the mean direction of the IG waves, none provides very accurate estimates. The BDM and the EMEP give closer estimations compared with the IMLM, but the BDM still produces false directional distribution in the opposite direction.

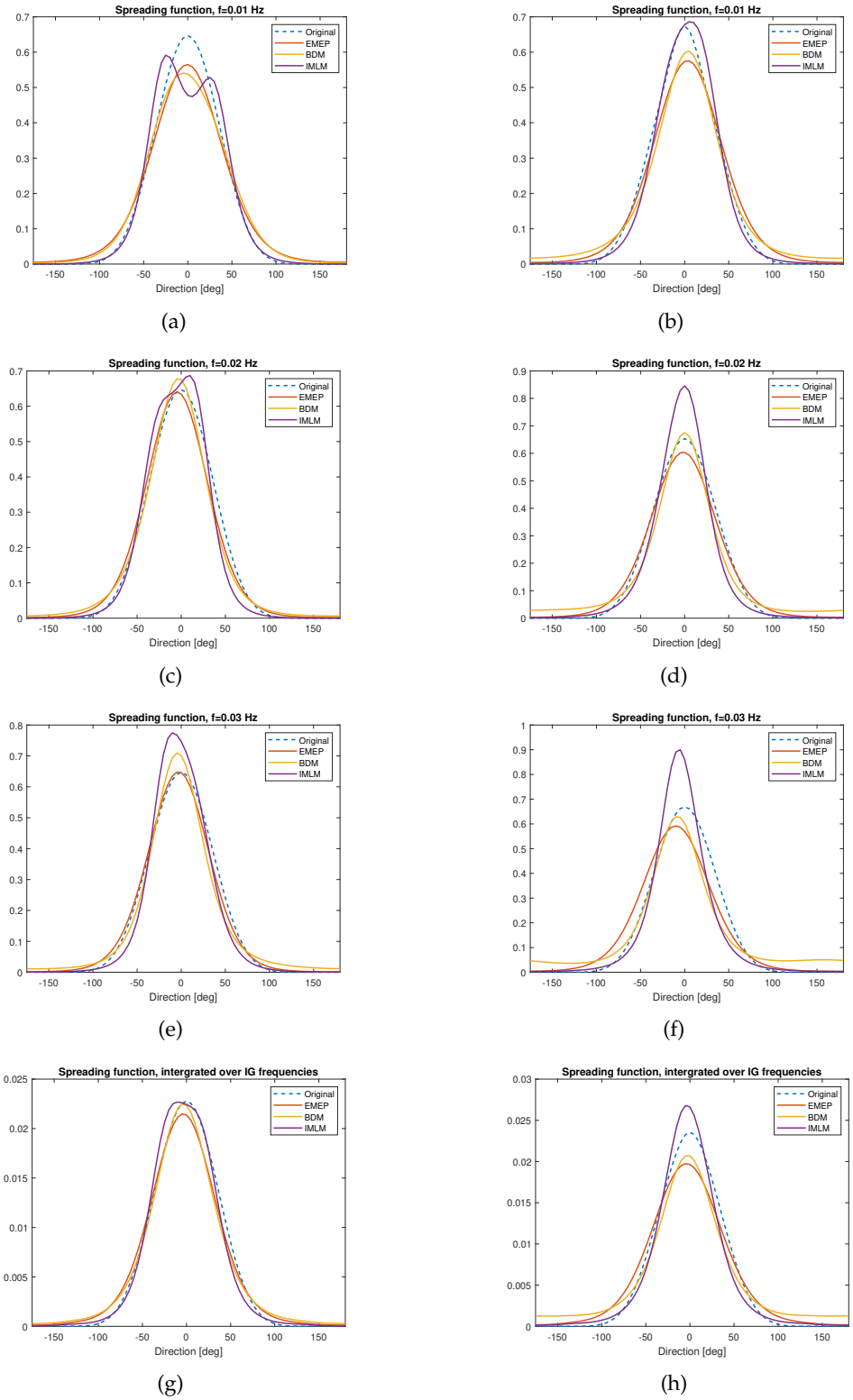

Figure 4.16: Analyzed results at different frequencies, compared with the original spectrum, $H_s = 2m, T_p = 8s$, water depth = 14m. Left: only free waves; Right: bound IG waves included, for original (dashed line), EMEP (red), BDM (yellow) and IMLM (blue).

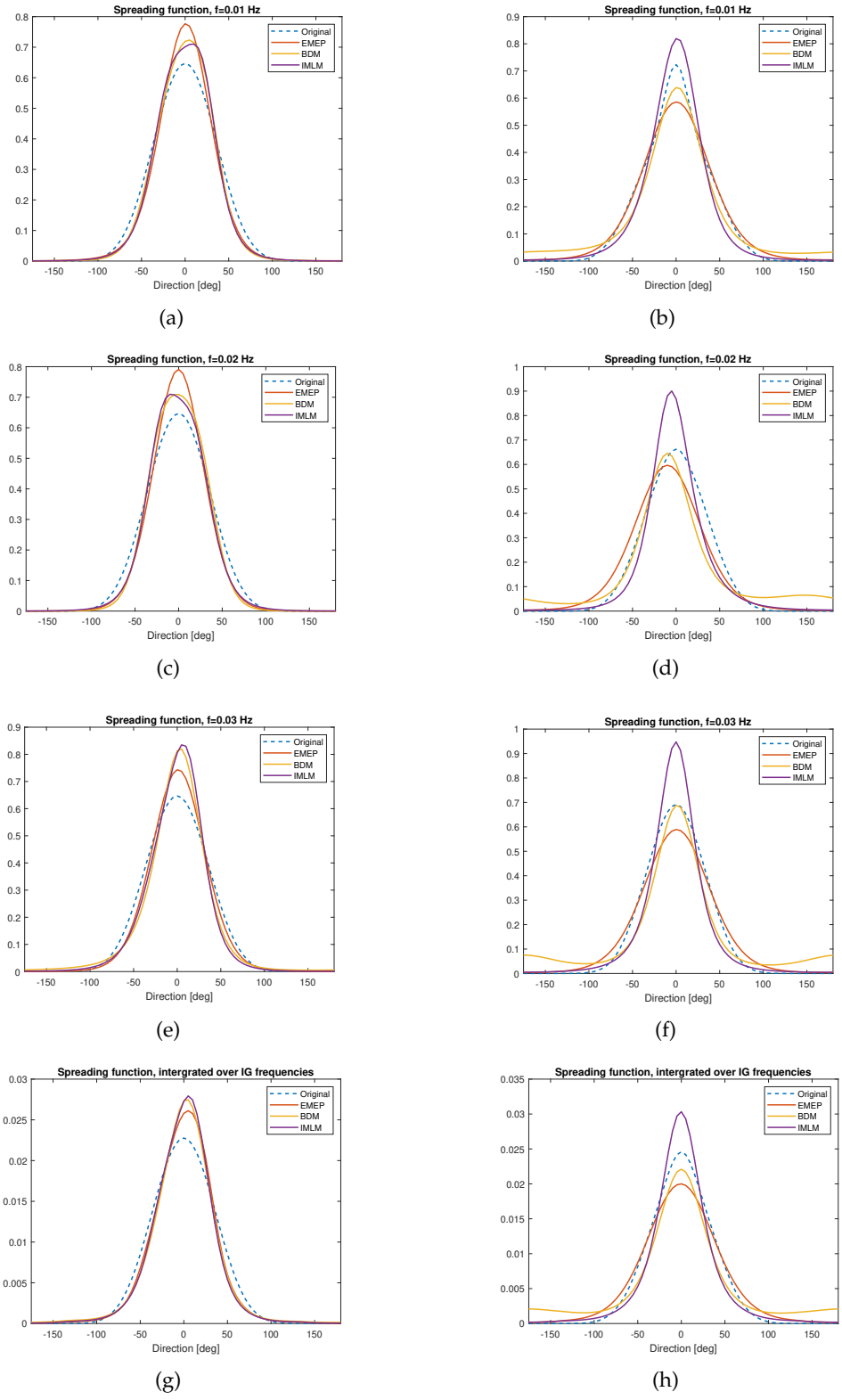

Figure 4.17: Analyzed results at different frequencies, compared with the original spectrum, $H_s = 4m, T_p = 8s$, water depth = 14m. Left: only free waves; Right: bound IG waves included, for original (dashed line), EMEP (red), BDM (yellow) and IMLM (blue).

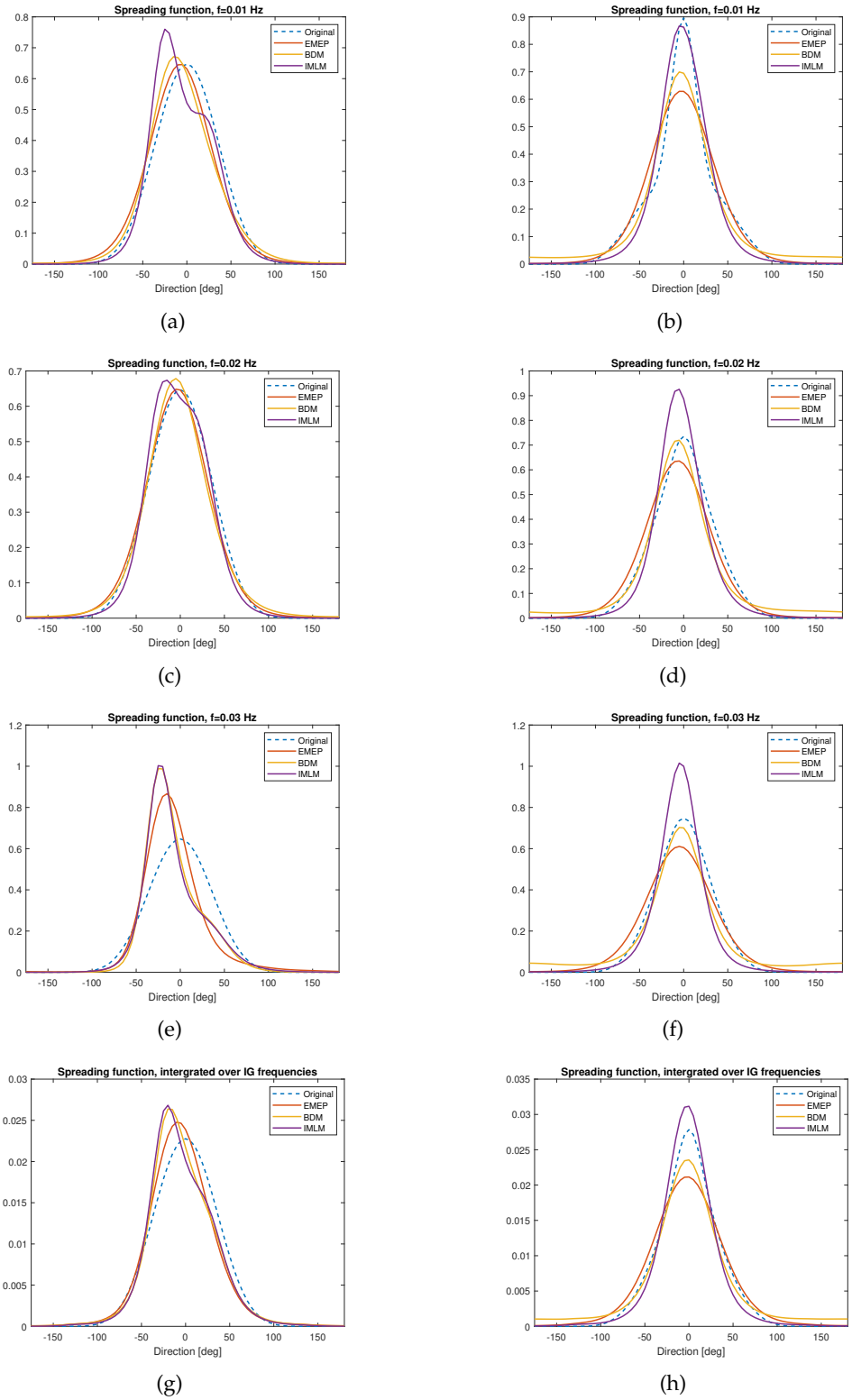

Figure 4.18: Analyzed results at different frequencies, compared with the original spectrum, $H_s = 4m, T_p = 8s$, water depth = 8m. Left: only free waves; Right: bound IG waves included, for original (dashed line), EMEP (red), BDM (yellow) and IMLM (blue).

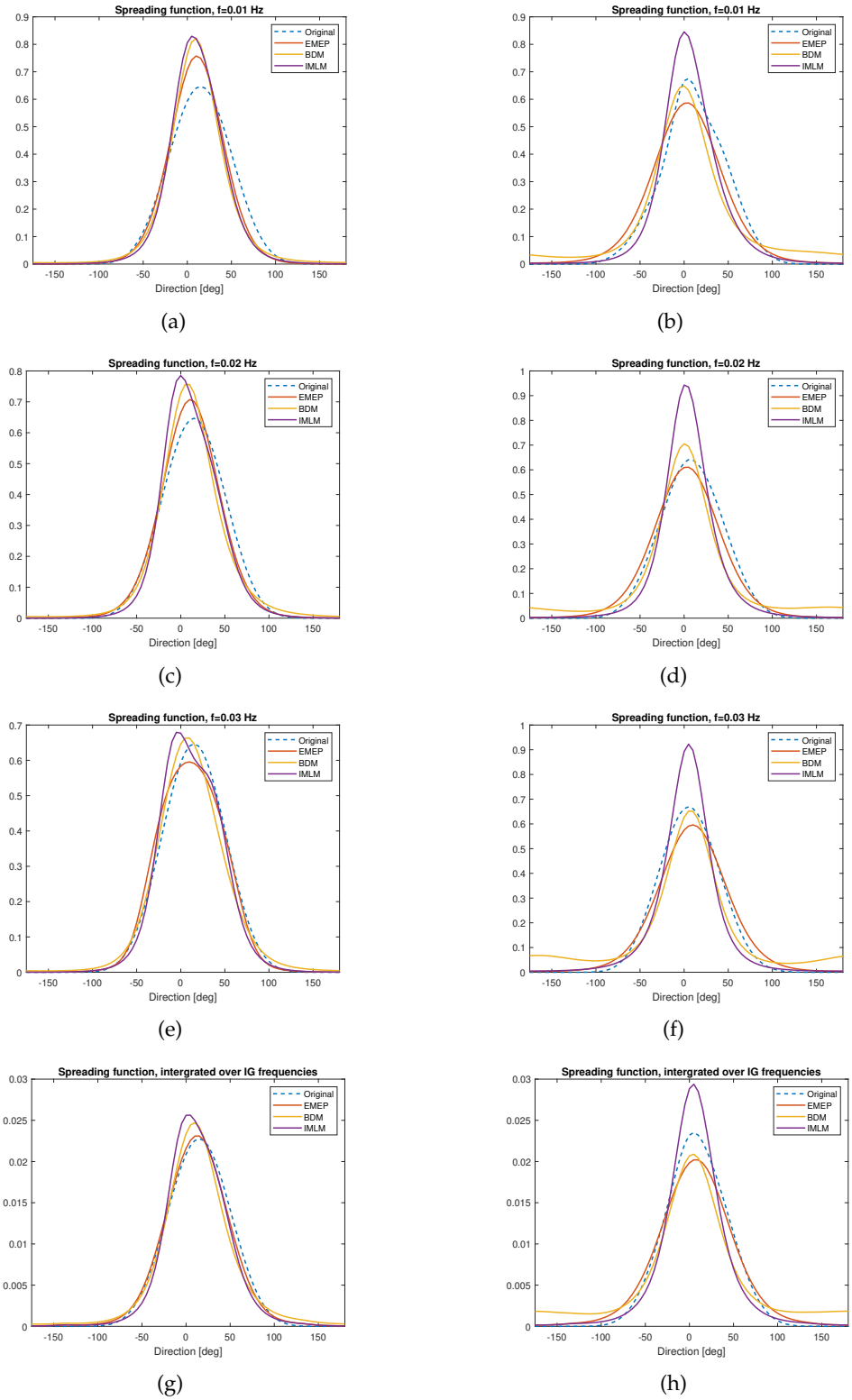

Figure 4.19: Analyzed results at different frequencies, compared with the original spectrum, $H_s = 3.25m, T_p = 8s$, water depth = 14m, mean direction of incident free IG waves is 15°. Left: only free waves; Right: bound IG waves included, for original (dashed line), EMEP (red), BDM (yellow) and IMLM (blue).

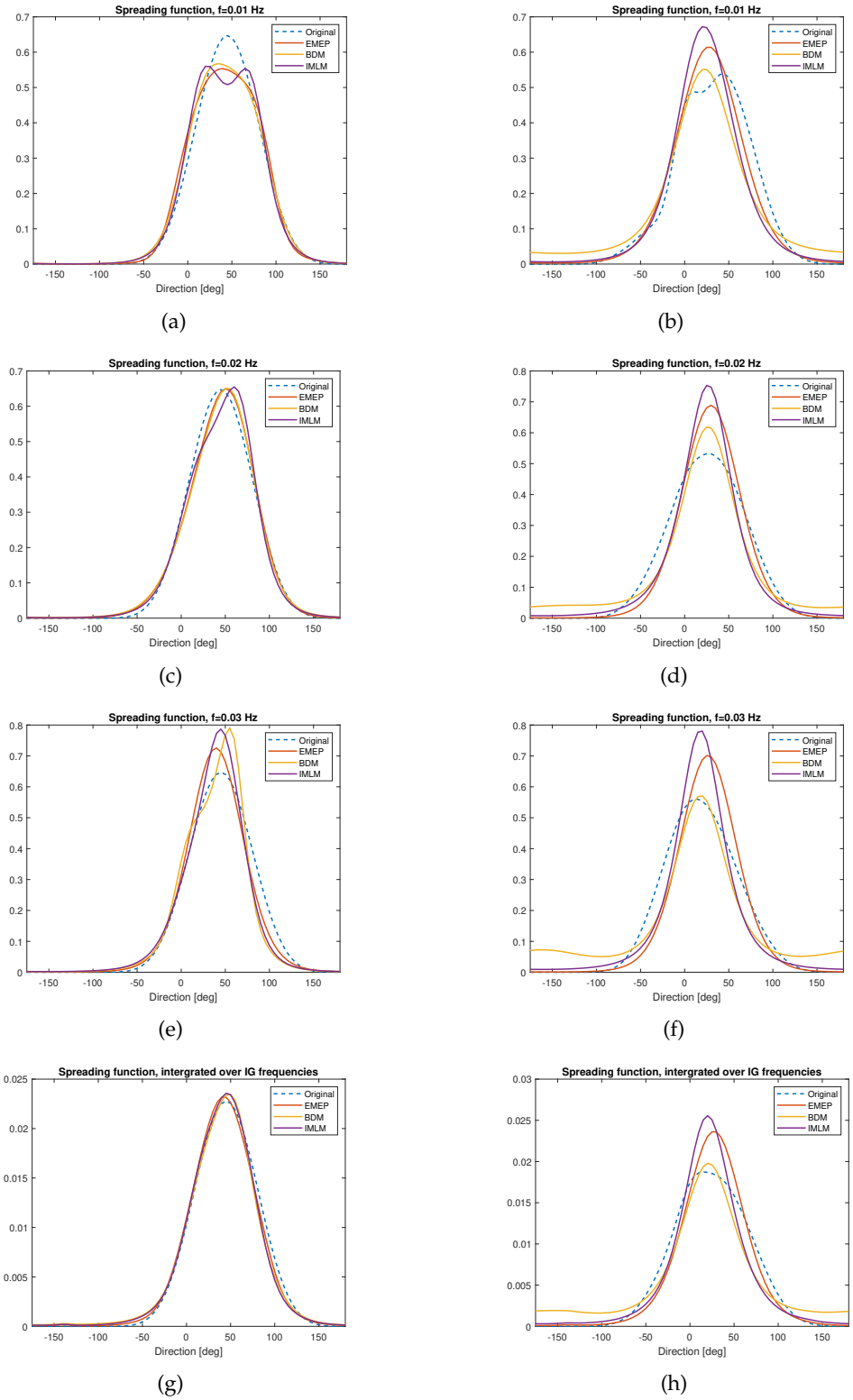

Figure 4.20: Analyzed results at different frequencies, compared with the original spectrum, $H_s = 3.25m, T_p = 8s$, water depth = 14m, mean direction of incident free IG waves is 45°. Left: only free waves; Right: bound IG waves included, for original (dashed line), EMEP (red), BDM (yellow) and IMLM (blue).

5 Discussion

5.1 Single-Point Systems

Three commonly used conventional directional wave spectra reconstruction methods are used to analyze artificial wave signals. The tests have shown that these methods usually estimate the directional wave spectra with acceptable accuracy. The wave signals are designed to simulate the REFLEX field wave conditions and can be regarded as recorded from ADCPs. The wave-related signals recorded by ADCPs can be used to reconstruct the directional wave spectra at their location. However, the EMEP and the BDM would have a more reliable performance when more signals are available. The BDM is designed for wave gauges arrays, and the EMEP performs less accurate when applied to a single-point system (Benoit et al., 1997). If obtaining the most accurate reconstructed wave spectra is the primary goal, wave gauge arrays might be used in the field to get more accurate, since they could provide more than three wave signals, even though they are harder to implement in the fields.

Additionally, in this report, we only use three wave components, the pressure signal remains unused. Although the ADCP can also record pressure signals, using four components seems cannot improve the quality of the estimates. For example, if we consider the first three test cases in Table 3.1, and compare the %error of the EMEP and the BDM reconstruction, we find that the results after analyzing pressure signals (measured from the bottom of the ADCP, 0.7m above the seafloor) are not more accurate than the original results, i.e., only consider three wave signals, water surface elevation and two orthogonal velocity components. See Table 5.1. Moreover, the IMLM cannot produce results after including pressure signals. More investigation are needed to find out the reason of these problems.

Case	EMEP(before)	EMEP(after)	BDM(before)	BDM(after)
1	5.1536	7.0503	10.5325	12.3460
2	7.0225	8.0057	11.6719	11.1993
3	6.7921	8.8835	57.7805	31.9955

Table 5.1: %Error of the EMEP and the BDM reconstruction for reference test cases, ”before” indicates the original results while ”after” indicates the results after considering pressure signals.

5.2 Energy Discrepancy between Spectral Parameters and Generated Spectra

The pre-defined directional spectra are generated based on several parameters, e.g., significant wave height and peak period, as introduced before. However, the wave energy contained in the generated spectrum may be somewhat different than the input parameters. The significant wave height of a pre-defined spectrum can be estimated simply based on the equation below:

$$H_s = 4\sqrt{m_0} \tag{5.1}$$

Where the 0-th moment of the pre-defined spectrum. The calculated wave height may be slightly higher or lower than the input wave height, the differences are often of order 1%.

This problem is minor for SS spectra estimation since the energy is significant at SS frequencies, but when considering the IG frequencies, which have much lower energy than the SS wave spectra, this energy discrepancy may lead to worse estimates.

5.3 Recommendations

In this report, three directional spectra reconstruction methods are tested using artificial wave signals. SS wave field, SS+IG wave field have been investigated, and the detailed DSF at IG frequencies is demonstrated. The methods have shown their ability to provide reasonable estimates when bound IG waves are included, even the wave condition is not moderate.

However, we only use artificial wave signals, which cannot fully represent the real conditions , e.g., in the REFLEX project. Multiple directional peaks may be expected in the fields, and the wave condition may be changeable during the storms. These concerns give more challenges when we interpret the field data. More investigations are needed to further validate and expand the findings in this report. More artificial wave signals, obtained from more complicated directional spectra, may be analyzed using the selected methods. It is also recommended that we use field data to examine these methods, by comparing the results from artificial data and actual data, we would get a better understanding of the directional properties of the IG wave fields.

6 Conclusions

In this study, three commonly used conventional directional wave spectra reconstruction methods, EMEP, IMLM and BDM, are compared. These methods have been broadly applied in the existing literature and coded in the open-source wave analysis toolbox DIWASP. Artificial wave signals were created to test the reliability and accuracy of these selected methods. Artificial wave signals were designed as if they were produced from the field measurements, since ADCPs were used in the field, water surface elevation and two orthogonal velocity components at 8m or 14m water depth are produced using a set of MATLAB codes.

This research followed the idea of van Essen et al. (2013) but particularly shows the detailed situation of the directional spreading function at IG frequency domains, and these methods may be used for the reconstruction of IG wave spectra.

The existence of bound waves weakens the performance of these estimation methods, in particular, the EMEP and the BDM are more reliable than the IMLM. However, the BDM may produce false directional distribution high wave height or narrow directional spreading, this leads to the recommendation of the EMEP, which was also recommended in van Essen et al. (2013).

No "best" method consistently produces better results than other methods, but overall, the reliability of the EMEP outperforms the other two methods since it provides fairly accurate estimates in any cases tested, the EMEP also has lower sensitivity to the changing parameters, compared to the BDM and the IMLM. The BDM, on the other hand, is accurate if the wave condition is calm or the directional spreading is broad. The IMLM tends to yield slightly narrower spectra than the target spectra, and often with a more significant %error than the EMEP does. The IMLM is hence not recommended if the EMEP is available.

Bibliography

Ardhuin, F., Rawat, A., and Aucan, J. (2014). A numerical model for free infragravity waves: Definition and validation at regional and global scales. *Ocean Modelling*, 77:20–32.

Benoit, M., Frigaard, P., and Schaffer, H. A. (1997). Analyzing multidirectional wave spectra: a tentative classification of available methods. *Proceedings of the 1997 IAHR conference*, (January 1997):131–158.

Benoit, M. and Goasguen, G. (1999). Comparative evaluation of directional wave analysis techniques applied to field measurements. In *The Ninth International Offshore and Polar Engineering Conference*. OnePetro.

Bertin, X., De Bakker, A., Van Dongeren, A., Coco, G., André, G., Ardhuin, F., Bonneton, P., Bouchette, F., Castelle, B., Crawford, W. C., et al. (2018). Infragravity waves: From driving mechanisms to impacts. *Earth-Science Reviews*, 177:774–799.

Brillouin, L. (1960). *Wave propagation and group velocity*, volume 8. Academic press.

Davidson, M. A., Huntley, D. A., and Bird, P. A. (1998). A practical method for the estimation of directional wave spectra in reflective wave fields. *Coastal engineering*, 33(2-3):91–116.

de Jong, M. P. C. and Borsboom, M. J. A. (2012). A Practical Post-Processing Method to Obtain Wave Parameters from Phase-Resolving Wave Model Results. *The International Journal of Ocean and Climate Systems*, 3:203–216.

Draycott, S., Davey, T., Ingram, D. M., Day, A., and Johanning, L. (2016). The SPAIR method: Isolating incident and reflected directional wave spectra in multidirectional wave basins. *Coastal Engineering*, 114:265–283.

Elgar, S., Herbers, T., Okihiro, M., Oltman-Shay, J., and Guza, R. (1992). Observations of infragravity waves. *Journal of Geophysical Research: Oceans*, 97(C10):15573–15577.

Hashimoto, N. (1997). Analysis of the directional wave spectrum from field data. In *Advances in coastal and ocean engineering*, pages 103–143. World Scientific.

Hashimoto, N. and Kobune, K. (1987). Estimation of directional spectra from a bayesian approach in incident and reflected wave field. *REPORT PORT & HARBOUR RES. INST.*, 26(4, Dec. 1987):3–33.

Hashimoto, N., Nagai, T., and Asai, T. (1994). Extension of the maximum entropy principle method for directional wave spectrum estimation. *Coastal Engineering Proceedings*, 1(24).

Hasselmann, K. (1962). On the non-linear energy transfer in a gravity-wave spectrum part 1. general theory. *Journal of Fluid Mechanics*, 12(4):481–500.

Hauser, D., Kahma, K. K., Krogstad, H. E., Lehner, S., Monbaliu, J., and Wyatt, L. W. (2005). Measuring and analysing the directional spectra of ocean waves. *Cost Office*, pages 80–83.

Herbers, T. H. C., Elgar, S., and Guza, R. T. (1994). Infragravity-frequency (0.005–0.05 hz) motions on the shelf. part i: Forced waves. *Journal of Physical Oceanography*, 24(5):917 – 927.

Herbers, T. H. C., Elgar, S., Guza, R. T., and O'Reilly, W. C. (1995). Infragravity-frequency (0.005–0.05 hz) motions on the shelf. part ii: Free waves. *Journal of Physical Oceanography*, 25(6):1063 – 1079.

Isobe, M. and Kondo, K. (1985). Method for estimating directional wave spectrum in incident and reflected wave field. In *Coastal Engineering 1984*, pages 467–483.

Johnson, D. (2002). Diwasp, a directional wave spectra toolbox for matlab®: User manual. *Center for Water Research, University of Western Australia*, pages 1–23.

Kuik, A. J., van Vledder, G. P., and Holthuijsen, L. H. (1988). A method for the routine analysis of pitch-and-roll buoy wave data. *Journal of Physical Oceanography*, 18(7):1020 – 1034.

Lashley, C. H., Bertin, X., Roelvink, D., and Arnaud, G. (2019). Contribution of infragravity waves to run-up and overwash in the pertuis breton embayment (france). *Journal of Marine Science and Engineering*, 7(7).

Munk, W. (1949). Surf beats. *EOS, Transactions American Geophysical Union*, 30(6):849–854.

Okihiro, M., Guza, R., and Seymour, R. (1992). Bound infragravity waves. *Journal of Geophysical Research: Oceans*, 97(C7):11453–11469.

Pawka, S. S. (1983). Island shadows in wave directional spectra. *Journal of Geophysical Research*, 88(C4):2579.

Plant, W. J. and Donelan, M. A. (2020). Directional surface wave spectra from point measurements of height and slope. *Journal of Atmospheric and Oceanic Technology*, 37(1):67–83.

Reniers, A. J., Naporowski, R., Tissier, M. F., de Schipper, M. A., Akrish, G., and Rijnsdorp, D. P. (2021). North sea infragravity wave observations. *Journal of Marine Science and Engineering*, 9(2):141.

Rijnsdorp, D. P., Reniers, A. J., and Zijlema, M. (2021). Free infragravity waves in the north sea. *Journal of Geophysical Research: Oceans*, 126(8):e2021JC017368.

van Dongeren, A., De Jong, M., Van der Lem, C., Van Deyzen, A., and Den Bieman, J. (2016). Review of long wave dynamics over reefs and into ports with implication for port operations. *Journal of Marine Science and Engineering*, 4(1):12.

van Essen, S., van der Hout, A., Huijsmans, R., and Waals, O. (2013). Evaluation of directional analysis methods for low-frequency waves to predict lngc motion response in nearshore areas. In *International Conference on Offshore Mechanics and Arctic Engineering*, volume 55317, page V001T01A015. American Society of Mechanical Engineers.

Waals, O. J. (2009). The effect of wave directionality on low frequency motions and mooring forces. In *International Conference on Offshore Mechanics and Arctic Engineering*, volume 43444, pages 289–298.